

Technical Report Documentation Page

1. Report No. FHWA/TX-07/0-1700-7		2. Government Accession No.		3. Recipient's Catalog No.	
4. Title and Subtitle Improvement of Portland Cement Concrete Pavement Performance				5. Report Date March 2007	
				6. Performing Organization Code	
7. Author(s) Chul Suh, Moon Won				8. Performing Organization Report No. 0-1700-7	
9. Performing Organization Name and Address Center for Transportation Research The University of Texas at Austin 3208 Red River, Suite 200 Austin, TX 78705-2650				10. Work Unit No. (TRAIS)	
				11. Contract or Grant No. 0-1700	
12. Sponsoring Agency Name and Address Texas Department of Transportation Research and Technology Implementation Office P.O. Box 5080 Austin, TX 78763-5080				13. Type of Report and Period Covered Research Report, 09/1999-08/2004	
				14. Sponsoring Agency Code	
15. Supplementary Notes Project performed in cooperation with the Texas Department of Transportation and the Federal Highway Administration.					
16. Abstract A general hydration model for cementitious materials and a model to predict the temperature gain in hardening concrete is developed and calibrated. A model to predict initial and final setting of hardening concrete is presented, and calibrated, with data collected under laboratory and field conditions. The effects of concrete temperature, different cements, and mineral admixtures on the initial and final times are characterized. Mathematical models were developed for the calculation of moisture and temperature profiles to help investigate the effect of different combinations of climate, construction, and materials on the development of the moisture and temperature profiles and their subsequent effects on early-aged cracking. The sensitivity of the design variables to the behavior of continuously reinforced concrete pavement (CRCP) has been investigated using mechanistic models of CRCP. The zero-stress temperature and the coefficient of thermal expansion of concrete are the most sensitive design variables, and the steel bar diameter and the vertical stiffness of underlying layers are the least sensitive variables. The effect of early opening to traffic on the life of portland cement concrete pavement systems was evaluated using experiments and mathematical model. A series of laboratory fatigue tests and accelerated fatigue tests on full-scale concrete slabs were performed. An analytical model for the numerical simulation for the prediction of the loss of life of a PCC pavement due to early opening was developed. The current opening criteria used by the Texas Department of Transportation appear to be reasonable based on the sensitivity analysis results.					
17. Key Words Concrete, CRCP, Early Age, Fatigue, Hydration, Moisture, Opening, Pavement, Temperature.			18. Distribution Statement No restrictions. This document is available to the public through the National Technical Information Service, Springfield, Virginia 22161; www.ntis.gov.		
19. Security Classif. (of report) Unclassified	20. Security Classif. (of this page) Unclassified	21. No. of pages 74		22. Price	



Improvement of Portland Cement Concrete Pavement Performance

Chul Suh
Moon Won

CTR Technical Report:	0-1700-7
Report Date:	March 2007
Project:	0-1700
Project Title:	Improvement of Portland Cement Concrete Pavement Performance
Sponsoring Agency:	Texas Department of Transportation
Performing Agency:	Center for Transportation Research at The University of Texas at Austin

Project performed in cooperation with the Texas Department of Transportation and the Federal Highway Administration.

Center for Transportation Research
The University of Texas at Austin
3208 Red River
Austin, TX 78705

www.utexas.edu/research/ctr

Copyright (c) 2007
Center for Transportation Research
The University of Texas at Austin

All rights reserved
Printed in the United States of America

Disclaimers

Author's Disclaimer: The contents of this report reflect the views of the authors, who are responsible for the facts and the accuracy of the data presented herein. The contents do not necessarily reflect the official view or policies of the Federal Highway Administration or the Texas Department of Transportation (TxDOT). This report does not constitute a standard, specification, or regulation.

Patent Disclaimer: There was no invention or discovery conceived or first actually reduced to practice in the course of or under this contract, including any art, method, process, machine manufacture, design or composition of matter, or any new useful improvement thereof, or any variety of plant, which is or may be patentable under the patent laws of the United States of America or any foreign country.

Engineering Disclaimer

NOT INTENDED FOR CONSTRUCTION, BIDDING, OR PERMIT PURPOSES.

Project Engineer: B. Frank McCullough
Professional Engineer License State and Number: Texas No. 19914
P. E. Designation: Research Supervisor

Acknowledgments

The researchers would like to acknowledge the expert assistance and guidance provided by the TxDOT project monitoring committee.

Research performed in cooperation with the Texas Department of Transportation and the U.S. Department of Transportation, Federal Highway Administration.

Products

This report contains the product 0-1700-P7, “Guidelines for Acceptance and Opening to Traffic Criteria for New PCC Pavements,” in the Appendix.

Table of Contents

Chapter 1. Introduction.....	1
1.1 Background.....	1
1.2 Objectives	1
1.3 Report Organization.....	1
Chapter 2. Temperature Control during Construction to Improve the Long-Term Performance of Portland Cement Concrete Pavement	3
2.1 Overview.....	3
2.2 Experimental Program	5
2.3 Hydration Model.....	6
2.3.1 Modeling of Early-Age Behavior and Temperature Development.....	6
2.3.2 Hydration of Cement-based Materials	8
2.3.3 Recommended General Hydration Model for Cementitious Materials	9
2.3.4 Temperature Prediction Program (PavePro).....	12
2.4 Temperature Model Calibration.....	12
2.5 Initial and Final Set of Concrete	13
2.6 Summary	14
Chapter 3. Moisture Related Cracking Effect on Concrete Pavement.....	15
3.1 Overview.....	15
3.2 Moisture-related Strength Factors in Concrete Pavements.....	15
3.3 Evaporation Modeling	16
3.4 Evaporation-induced Cracking	17
3.4.1 Sensitivity of Moisture to Delamination Stress	18
3.4.2 Wind Speed, Curing Quality, and Aggregate Bond.....	19
3.5 Summary	21
Chapter 4. Sensitivity Analysis of CRCP Computer Programs	23
4.1 Overview.....	23
4.1.1 Background.....	23
4.1.2 Objectives	23
4.1.3 Approach.....	24
4.2 Input Variables.....	24
4.3 Sensitivity Analysis Results.....	24
4.3.2 General Observations.....	26
4.3.3 Concrete Properties.....	26
4.3.4 Steel Properties	27
4.3.5 Slab/Subbase Resistance.....	27
4.3.6 External Wheel Loads.....	28
4.3.7 Climatic Loads.....	28
4.3.8 Summary of Sensitivity.....	28
4.4 Summary	30
Chapter 5. The Effect of Early Opening to Traffic.....	31
5.1 Overview	31

5.1.1 Objectives	31
5.1.2 Approach and Scope	31
5.2 Concrete Materials	32
5.3 Laboratory Beam Fatigue Testing	32
5.3.1 Laboratory Specimens	32
5.3.2 Laboratory Fatigue Testing Procedures	33
5.3.3 Laboratory Fatigue Testing Results	33
5.4 Super-accelerated Slab Testing	35
5.4.1 Description of Stationary Dynamic Deflectometer (SDD)	36
5.4.2 Foundation Properties	37
5.4.3 Full-Scale Concrete Slab Properties	37
5.4.4 Super-Accelerated SDD Slab Testing Procedure	39
5.4.5 Super-Accelerated Full-Scale Concrete Slab Testing Results	43
5.5 Opening-to-Traffic Flexural Strength Criteria	47
5.5.1 Mathematical Model	47
5.5.2 Regression Analysis	49
5.6 Summary	54
Chapter 6. Conclusions	55
6.1 Temperature Control	55
6.2 Moisture Effects	55
6.3 Sensitivity Analysis of CRCP Computer Program	55
6.4 Early Opening Criteria	56
Appendix: Guidelines for Acceptance and Opening to Traffic Criteria for New PCC Pavements.	57
References	59

List of Figures

Figure 2.1: Overview of research strategy	4
Figure 3.1: Sensitivity study for delamination stress.....	19
Figure 3.2: Effect of wind speed on delamination stress	20
Figure 5.1: Summary of laboratory beam fatigue testing	34
Figure 5.2: Illustrations of SDD testing method	35
Figure 5.3: General SDD testing arrangement.....	36
Figure 5.4: Photographs of foundation testing at the full-scale slab testing.....	38
Figure 5.5: Static and dynamic instrumentation	40
Figure 5.6: Photograph of field arrangement of SDD super-accelerated testing.....	41
Figure 5.7: Photograph of full-scale slab fatigue testing in progress	42
Figure 5.8: Photographs of failed slabs after fatigue testing	45
Figure 5.9: Variation of normalized dynamic displacement for full-scale slabs	46
Figure 5.10: Comparison of laboratory beam and full-scale slab fatigue curves	47
Figure 5.11: Conceptual diagram of the loss of life.....	49
Figure 5.12: Sensitivity analysis of required flexural strength for opening with various subgrade reaction modulus (interior loading condition).....	52
Figure 5.13: Sensitivity analysis of required flexural strength for opening with various edge loading ratio ($k = 300$ pci).....	53

List of Tables

Table 2.1: ASTM C 1074 activation energy values obtained from compressive strength data.....	6
Table 2.2: The effect of different parameters on the general hydration model	10
Table 3.1: Typical values of parameters of delamination model.....	18
Table 4.1: Summary of low, medium, and high values of each variable.....	25
Table 4.2: Sensitivity of design variables	29
Table 5.1: Mixture proportions	32
Table 5.2: Super-accelerated full-scale slab fatigue testing results	43
Table 5.3: Summary of used input variables	50

Chapter 1. Introduction

1.1 Background

Both directly and through sponsored research, Texas Department of Transportation (TxDOT) has been monitoring the condition of the state's rigid pavements for more than 25 years (Dossey et al., 1994). Due to that effort, it is now well established that Portland Cement Concrete (PCC) pavements will provide 25-40 years of service on high volume roadways with minimum maintenance if designed and built correctly. However, it is also equally clear that some PCC pavements have suffered a high rate of failure development for various reasons, causing them to fail far short of their design life—by as much as 50%. These problem pavements continue to be constructed, resulting in unnecessary expense and inconvenience to the public.

Much work has been done over the past decade to determine the causes for these early failures. Many of the pertinent issues in pavement design, pavement materials, and construction practices related to long-term PCC pavement performance have already been examined to some degree. Findings from these studies have indeed resulted in a better understanding of how PCC pavements behave under various environmental and traffic conditions. What is needed now is a comprehensive plan to coordinate research and implementation to address this problem, encompassing design, construction, specifications, and testing elements to ensure high performance from all PCC pavements.

1.2 Objectives

The primary objective of this study was to develop procedures to improve the long-term performance of concrete pavements. In order to achieve the primary objective, several task objectives were required during this study. The following list briefly itemizes the main objectives of this research program:

- 1) Develop a procedure for temperature control during construction to improve the long term performance of PCC pavement
- 2) Evaluate the effects of moisture loss on strength and spalling development
- 3) Maximize the accuracy and reliability of the CRCP-10 program
- 4) Evaluate the early opening criteria of PCC pavements to traffic
- 5)

1.3 Report Organization

This report is organized into six chapters, including the current, introductory Chapter 1. Following is a brief description of Chapters 2 through 6.

Chapter 2 describes the development of a procedure for temperature control. Chapter 3 presents moisture related cracking effects on PCC pavements. Chapter 4 provides the results of the initial steps in the process of maximizing the accuracy and reliability of the CRCP-10 program. (CRCP refers to *continuously reinforced concrete pavement*). Chapter 5 presents the

evaluation for the early opening criteria of PCC pavements to traffic. Finally, Chapter 6 provides overall summary and conclusions of this study. The appendix contains the guidelines for acceptance and opening to traffic criteria for new PCC pavements.

Chapter 2. Temperature Control during Construction to Improve the Long-Term Performance of Portland Cement Concrete Pavement

2.1 Overview

High concrete temperatures increase the rate of hydration, thermal stresses, the tendency for drying shrinkage cracking, and permeability, which decreases long-term concrete strength and durability due to the cracking. Findings from past research efforts have demonstrated that the concrete temperature development during the first 24 to 72 hours has a major impact on long-term pavement performance (Hankins et al., 1991; Dossey et al., 1994; and McCullough et al., 1998). Excessive portland cement concrete (PCC) temperature development may result in reduced pavement performance. All these factors emphasize that concrete temperature control during construction in hot weather conditions is essential to improve the durability of PCC pavements.

The long-term temperature change the pavement is subjected to, and the aggregate type used during construction, largely determine the long-term stabilized crack distribution in continuously reinforced concrete (CRC) pavements. Current CRC pavement reinforcement design practice involves the selection of a long-term temperature change to obtain the reinforcement amount best suited for the pavement under design. However, no attempt is made during construction to ensure that the design long-term temperature change is not exceeded under field conditions. This is analogous to not having weight limits on bridges to guard against overloading. Longer-lasting concrete pavements will be produced if the assumptions made during design are not exceeded in the field.

Most states specify a maximum concrete temperature at placement, and the limit remains the same irrespective of the type of mineral or chemical admixtures used. In modern paving operations, the use of mineral admixtures has become common practice, and under certain conditions, these admixtures could mitigate some of the problems associated with hot weather placement. Furthermore, the use of a maximum concrete placement temperature does not address long-term performance issues, as the maximum in-place concrete temperature remains uncontrolled. Through the appropriate selection of construction materials and construction practices, the detrimental effects of hot weather concreting can be countered. However, in order to control the in-place temperature, the variables that influence it most need to be identified and their effect quantified.

The focus of work in this chapter (Shindler et al., 2002) is to develop procedures to improve the long-term performance of concrete pavements, especially when constructed under hot weather conditions. This section outlines the research undertaken during the course of this study. In this section, the objectives of this study, the significance of the work, and the research plan for this study are presented.

The primary objective of this study is to develop procedures to improve the long-term performance of concrete pavements, especially when constructed under hot weather conditions.

The temperature prediction program developed in this study will allow pavement designers and contractors to quantify and evaluate the effect of various controllable and uncontrollable parameters on the in-place temperature development. In order to investigate the

hydration characteristics of typical Texas paving mixtures, different concrete paving mixtures were tested by semi-adiabatic calorimeter testing. A database was developed of test results and all the known variables for these mixtures, which was then evaluated to characterize the hydration of different cementitious systems.

The overall research strategy of this section is schematically outlined in Figure 2.1. The approach will involve the development of an end-result type specification, which limits the maximum in-place concrete temperature of the hydrating concrete. The specified values should be based on the amount of reinforcement provided in the section, the project location, and the type of coarse aggregate used in the concrete mixture. This practice would thus link the design conditions to the actual construction conditions experienced on site. The temperature prediction program functions as a tool for contractors and designers to evaluate and compare different options that might lower the in-place concrete temperature.

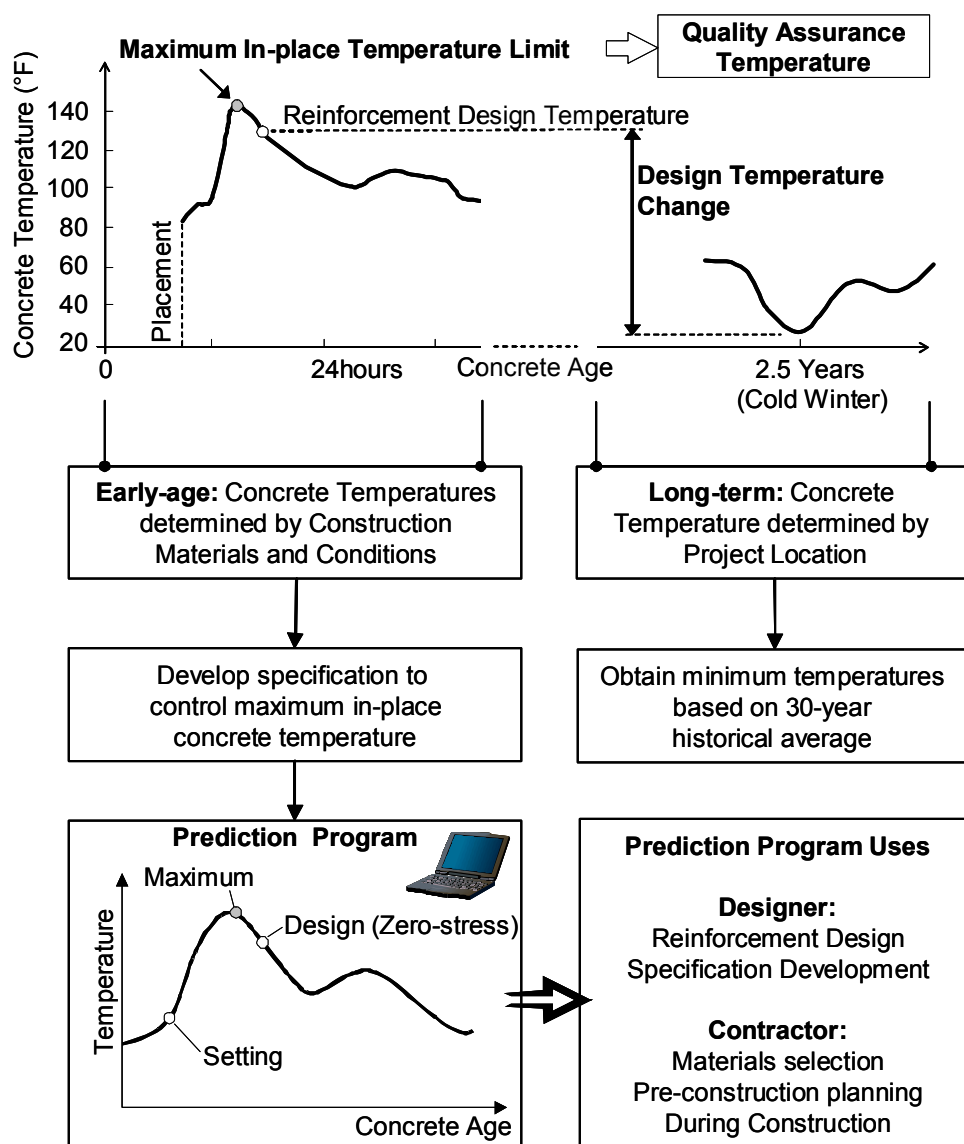


Figure 2.1: Overview of research strategy

2.2 Experimental Program

Numerous factors affect the development of the in-place concrete temperatures, and it is essential with any mechanistic model that local materials are tested to calibrate it for local conditions. The calibration requires actual test data, and the more detailed and comprehensive this data set, the higher the confidence in the calibrated model.

All the materials and concrete mixtures were selected to be representative of concrete paving mixtures in the state of Texas. Data were collected from the following three phases: (1) field work, (2) materials characterization, (3) concrete hydration under controlled conditions.

Seven field sites were instrumented in three Texas cities: Dallas, Houston, and El Paso. The variables that were collected include the mixture design properties, concrete properties, concrete temperature history, environmental conditions during placement, pavement thickness, subbase type, subbase temperature, and curing methods used. At each site, raw materials were collected for laboratory testing. The in-place concrete temperatures are presented in this chapter. The highest concrete temperature of 144°F was measured in a section placed under summer conditions in Dallas. While on site, the adverse effects of placing concrete in hot weather conditions were clearly noticeable. Concrete setting occurred very quickly, and the window of opportunity for tining was very small and in some instances, the specified surface tining could not be achieved, because the concrete was already too hard. Portions of the pavement placed on this project showed significant plastic shrinkage cracking.

The time of setting with the penetration resistance method (ASTM C 403) was successfully determined on site. A portable vibration table was used to sieve the concrete mixture through the #4 sieve to obtain the mortar sample. Setting tests were performed on the same mixtures under laboratory conditions. The activation energy for 21 different mixtures as per ASTM C 1074 was determined during this study. The activation energy of each of the mixtures was obtained based on the best-fit slope of the Arrhenius plot. As ASTM C 1074 only provides recommendations when Type I mixtures are used, the values in Table 2.1 may be a useful reference when activation energy values are required for mixtures with cements other than Type I.

Because this method is currently used by TxDOT, Table 2.1 might serve as a guide for the selection of an appropriate datum temperature value for the specific mixture under consideration.

In order to investigate the hydration characteristics of typical Texas paving mixtures, 21 different concrete paving mixtures were tested by semi-adiabatic calorimeter testing. A database of test results and all the known variables was developed for these mixtures. The degree of hydration data collected during this project will be useful to obtain a better understanding of the hydration of cementitious materials made from different mixture proportions, cement chemical composition, and mineral admixtures.

Small insulated concrete slabs were cured under enclosed and controlled laboratory conditions. This process minimizes the impact climatic conditions such as fluctuating wind speeds, cloud cover, air temperatures, and fluctuating relative humidity. The effect of solar radiation on the development of concrete temperatures is removed under these conditions.

Table 2.1: ASTM C 1074 activation energy values obtained from compressive strength data

Mix No.	Description	Datum Temperature * (°F)	Activation Energy (J/mol)	
			Hyperbolic	Exponential
1	Type I/II + 20% Class F fly ash	30.2	31,062	38,359
2	Type I/II + 25% Class C fly ash	41.2	40,914	38,671
3	Type I	30.4	31,486	42,081
4	Type I/II + 35% Class C fly ash	29.7	32,370	35,121
5	Type I/II + 50% GGBF Slag	25.9	29,597	38,400
6	Type I/II + 20% Class F fly ash	30.2	30,565	40,790
7	Type I/II + 25% Class C fly ash	41.4	46,854	41,254
8	Type I + 30% Class C fly ash	15.1	32,920	36,459
9	Type I Cement	36.7	38,985	42,330
10	Type I + 15% Class C Fly Ash	32.0	36,953	46,628
11	Type I + 25% Class C Fly Ash	26.4	32,361	44,249
12	Type I + 35% Class C Fly Ash	32.5	34,976	41,283
14	Type I + 15% Class F Fly Ash	33.6	42,470	47,003
15	Type I + 25% Class F Fly Ash	35.6	39,731	49,378
16	Type I + 35% Class F Fly Ash	30.9	32,556	45,017
18	Type I + 30% GGBF Slag	33.1	31,964	33,415
19	Type I + 50% GGBF Slag	33.6	39,415	43,374
20	Capitol Type I	34.5	34,938	38,147
21	Alamo Type I	18.0	25,215	39,221

Note: * Determined in accordance with ASTM C 1074, and the hyperbolic function

2.3 Hydration Model

2.3.1 Modeling of Early-Age Behavior and Temperature Development

This section documents the assembly of the models necessary to predict the in-place temperature development, setting, and stresses of concrete at early-ages. Models were selected to simulate the factors that influence the development of concrete temperatures, and the hydration of cementitious material. During the selection of the models, compatibility was kept in mind in order to ensure that the overall model can be developed.

The key element of this study involved the development of a temperature prediction program to characterize and quantify the early-age temperature development in hardening

concrete. As part of this effort, general hydration models were developed to characterize the heat of concrete hydration for different cementitious materials and mixture proportions. The model was developed from 34 different mixtures, made from 23 different cements. The model considers the effect of cement chemical composition, cement fineness, mineral admixtures (fly ash, and GGBF slag), mixture proportions, and concrete properties.

It is essential with any mechanistic empirical model, that local materials are tested and the models are calibrated for local conditions. It is proposed that the models be calibrated with laboratory data in a controlled environment, and with field measurements. The final step should be the validation of the model based on another set of independent field measurements.

The work documented in this section presents mechanistic models to determine the heat transfer from the pavement system to the environment. A number of models are presented in detail and the models will be calibrated later in this report. It is recommended that the models be evaluated for implementation into the temperature prediction program.

The early-age temperature development of concrete could be estimated from knowledge of cement the composition, cement fineness, the presents of admixtures, thermal characteristics of the concrete (aggregate type) and surroundings, the slab thickness, and the prevailing environmental conditions. Numerous factors are involved and the fact that most of these factors do not influence the concrete temperature independent of each other, and the use of adiabatic testing will be necessary to determine the internal heat generated by local concretes.

Models were selected to characterize the factors that have the most significant influence on the development of concrete temperatures. The most applicable models were selected, and compatibility of all the available models was kept in mind in order to ensure that the overall model can be developed. The proposed model could account for the following factors: cement composition, water-cement ratio, cement fineness, mineral admixtures, initial concrete temperature at placement, environmental conditions, subbase temperature, and slab thickness.

Techniques are available from literature to predict the heat transfer from the concrete to the surroundings; however, the development of a computer program to facilitate the computing process will be required. Heat transfer through conduction, convection, irradiation, and solar absorption can account for the effects of different in-place conditions.

High zero-stress temperatures will increase the thermal stresses the pavement is subject to over its intended life. Temperature control in pavements is thus related to the control and minimization of excessive zero-stress temperatures, which have been shown to produce poor long-term pavement performance.

Few models are available to characterize the time-dependent deformation and creep compliance of concrete at very early-age (less than 2 days). It is recommended that the Extended Triple Power Law as developed by Westman (1999) be developed and evaluated to account for early-age relaxation effects. This model is recommended because it accounts for the following factors that could influence the time-dependent deformation: concrete age at setting, concrete age at loading (including ages less than 2 days), applied stress level, and the influence of varying temperature on concrete properties.

Based on the information reviewed and presented in this document, it is evident that many models are available to predict the concrete temperature. However, due to the nature of any mechanistic model, and the fact that most of the literature available was conducted outside of the United States, calibration for local conditions and materials will be an essential phase to ensure that the models are valid under the intended conditions.

2.3.2 Hydration of Cement-based Materials

The hydration of different cementitious systems can be characterized by the mechanistic-empirical models developed during this study. It is shown that the explanatory variables are statistically significant. The model provides a reasonable and accurate representation of the in-place temperature development of concrete pavements.

The hydration model uses the activation energy with the equivalent age maturity method to define the temperature sensitivity of the hydration process. The degree of hydration characterizes the formation of hydration products as hydration progresses over time, and each concrete mixture has a unique degree of hydration development. Based on the temperature sensitivity (activation energy), the degree of hydration at the reference temperature, and the total heat of hydration, the heat of hydration of a concrete mixture can accurately be characterized. Conclusions regarding the temperature sensitivity and degree of hydration model will be discussed separately.

Temperature Sensitivity (Activation Energy)

This document presents evidence from various sources that different activation energy values should be used when mechanical properties and the development of hydration (chemical effects) are considered. The crossover effect develops only when mechanical properties are considered and not when the degree of hydration development is considered. The activation energy determined with the ASTM C 1074 should not be used to define the temperature sensitivity of the cement hydration process.

In all the cases investigated, the data indicated that the heat of hydration data obeys the Arrhenius principle, as the activation energy was determined to be independent of the hydration temperature.

The slope of the Arrhenius plot is influenced by the chemical composition of the cement and the use of mineral admixtures. The activation energy for different cements ranged from 36,132 J/mol to 54,467 J/mol. A multivariate nonlinear statistical analysis indicated that the change in activation energy might be modeled in terms of the Blaine value, the C₃A content, and the C₄AF content of the cement. The hydration at different temperatures can accurately be predicted through the equivalent age maturity method and the use of an experimentally determined constant activation energy.

Concrete Hydration Development

A mechanistic-empirical model is proposed to characterize the heat of hydration of concrete at an isothermal curing temperature of 70°F (21.1°C). The model considers the effect of:

- Cement chemical composition: C₃A, C₃S, C₂S, C₄AF, SO₃, MgO, and Free Lime
- Cement fineness: specific surface area (Blaine Index)
- Mineral admixtures: Class F fly ash, Class C fly ash, and GGBF slag
- Mixture proportions: cement content, water-cementitious ratio, mineral admixture replacement level, coarse aggregate content, and fine aggregate content
- Concrete properties: density, thermal conductivity, specific heat

Based on the data reviewed and analyzed in this study the following conclusions can be made:

- Semi-adiabatic testing provides a convenient indirect means to characterize the formation of hydration products by measuring the heat released during hydration.
- The development of the degree of hydration is influenced by the cement chemical composition, the cement fineness, the use of mineral admixtures, and the mixture proportions used in the concrete mixture. The effect of each parameter is summarized in Table 2.2.
- Results from semi-adiabatic tests revealed that complete hydration does not occur in any of the concretes tested. This is attributed to the low water-cement ratios used in the concretes tested. This directly affected the total amount of heat released during hydration.
- The ultimate degree of hydration is unaffected by the curing temperature. The ultimate degree of hydration appears to be increased when fly ash or GGBF slag is used.

2.3.3 Recommended General Hydration Model for Cementitious Materials

In this section, all the recommended components are presented in a concise format. The degree of hydration is expressed with the following exponential function:

$$\alpha(t_e) = \alpha_u \cdot \exp\left(-\left[\frac{\tau}{t_e}\right]^\beta\right) \quad (2.1)$$

where

- $\alpha(t_e)$ = the degree of hydration at equivalent age, t_e ,
- τ = hydration time parameter (hrs),
- β = hydration shape parameter, and
- α_u = ultimate degree of hydration

The rate of heat liberation is defined as follows:

$$Q_h(t) = H_u \cdot C_c \cdot \left(\frac{\tau}{t_e}\right)^\beta \cdot \left(\frac{\beta}{t_e}\right) \cdot \alpha(t_e) \cdot \frac{E}{R} \left(\frac{1}{273+T_r} - \frac{1}{273+T_c} \right) \quad (2.2)$$

where

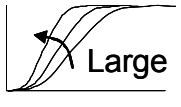


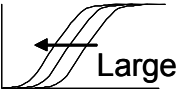


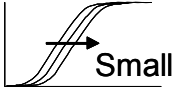
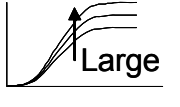
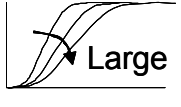

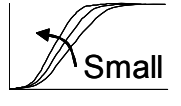

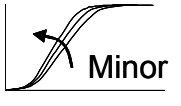
- $Q_h(t_e)$ = rate of heat liberation at equivalent age, t_e , (W/m³),
- C_c = cementitious materials content (g/m³), and
- H_u = total heat of hydration of cementitious materials at 100% hydration (J/g), defined as:

$$H_u = H_{cem} \cdot p_{cem} + 461 \cdot p_{SLAG} + 1800 \cdot p_{FA-CaO} \cdot p_{FA}$$

where

- p_{SLAG} = slag mass ratio to total cementitious content,
- p_{FA} = fly ash mass ratio to total cementitious content,
- p_{FA-CaO} = fly ash CaO mass ratio to total fly ash content,
- p_{cem} = cement mass ratio to total cementitious content, and
- H_{cem} = heat of hydration of the cement, defined by (Bogue, 1947) as:

Table 2.2: The effect of different parameters on the general hydration model

Parameter	Value	See Figure	Effect on Degree of Hydration		
			Start of Acceleration Phase	Rate (Slope)	Ultimate Value
C_3A	↑	5-60	-	 Large	-
C_3S	↑	5-59	-	 Medium	-
SO_3	↑	5-61	-	 Very Large	-
Cement Fineness: (Blaine Value)	↑	5-57 and 5-58	 Large	 Large	-
Class F fly ash dosage	↑	5-63	-	-	 Large
Class C fly ash dosage	↑	5-64	 Small	-	 Large
GGBF slag dosage	↑	5-65	-	 Large	 Large
w/cm ratio	↑	5-62	-	 Small	 Large
Alkalies*	↑	5-66	-	 Minor	-

Note: *Alkalies are indirectly considered through the SO_3 content

$$H_{cem} = 500 \cdot p_{C_3S} + 260 \cdot p_{C_2S} + 866 \cdot p_{C_3A} + 420 \cdot p_{C_4AF} + 624 \cdot p_{SO_3} + 1186 \cdot p_{FreeCa} + 850 p_{MgO} \quad (2.3)$$

where

p_i = mass ratio of i-th component to total cement content.

A multivariate nonlinear regression model was developed based on heat of solution, conduction calorimeter, and semi-adiabatic calorimeter test data. An r^2 of 0.988 was achieved with this model. At the isothermal curing temperature of 21.1°C, the recommended model is as follows:

$$\tau = 66.78 \cdot p_{C_3A}^{-0.154} \cdot p_{C_3S}^{-0.401} \cdot Blaine^{-0.804} \cdot p_{SO_3}^{-0.758} \exp(2.187 \cdot p_{SLAG} + 9.50 \cdot p_{FA} \cdot p_{FA-CaO}) \quad (2.4)$$

$$\beta = 181.4 \cdot p_{C_3A}^{0.146} \cdot p_{C_3S}^{0.227} \cdot Blaine^{-0.535} \cdot p_{SO_3}^{0.558} \cdot \exp(-0.647 \cdot p_{SLAG}) \quad (2.5)$$

$$\alpha_u = \frac{1.031 \cdot w/cm}{0.194 + w/cm} + 0.50 \cdot p_{FA} + 0.30 \cdot p_{SLAG} \leq 1.0 \quad (2.6)$$

where

- p_{C_3A} = weight ratio of tricalcium aluminate to total cement content,
- p_{C_3S} = weight ratio of tricalcium silicate to total cement content,
- p_{SO_3} = sulfate weight ratio to total cement content,
- $Blaine$ = Blaine value, specific surface area of cement (m²/kg), and
- w/cm = the water-cementitious material ratio.

The temperature sensitivity of the hydration process was evaluated based on heat of solution and conduction calorimeter tests data. The tests were performed over a temperature range of 40°F (4.4°C) to 105°F (40.6°C). The best-fit activation energy (E) model was developed and found to be independent of curing temperature. This is in agreement with the Arrhenius theory for rate processes in chemical reactions. The recommended activation energy model is defined as follows:

$$E = 22,100 \cdot f_E \cdot p_{C_3A}^{0.30} \cdot p_{C_4AF}^{0.25} \cdot Blaine^{0.35} \quad (2.7)$$

where

- p_{C_3A} = weight ratio of tricalcium aluminate Bogue compound,
- p_{C_4AF} = weight ratio of tetracalcium aluminoferrite Bogue compound,
- $Blaine$ = Blaine value, specific surface area of cement (m²/kg), and
- f_E = Activation energy modification factor, defined as:

$$f_E = 1 - 1.05 \cdot p_{FA} \cdot \left(1 - \frac{p_{FACaO}}{0.40} \right) + 0.40 \cdot p_{SLAG} \quad (2.8)$$

where

- p_{FA} = Mass ratio replacement of the fly ash,
- p_{FACaO} = Mass ratio of the CaO content in the fly ash, and
- p_{SLAG} = Mass ratio replacement of the GGBF Slag.

2.3.4 Temperature Prediction Program (PavePro)

One of the key objectives of this study was to quantify the effect of different materials and construction practices on the development of concrete temperatures. A temperature prediction program was developed. The program was successfully calibrated for the variables that may have a significant impact on the in-place concrete temperature. It may be concluded that the proposed temperature prediction model could be used as a tool (design aid) to evaluate the following parameters:

- different cement contents,
- cement composition,
- water-cement ratio,
- cement fineness,
- the use of Class F and C fly ash,
- the use of GGBF slag,
- initial concrete temperature at placement,
- environmental conditions,
- curing methods,
- subbase temperature,
- pavement thickness, and
- time of placement.

The temperature prediction model will enable the designer and contractor to evaluate, in a short time frame, the effect of the different options on the predicted in-place concrete temperature development. The temperature prediction model enables the development of performance-based specifications to guard against premature concrete failures. The model can be used to determine the most effective combination of materials and construction operations to ensure that the reinforcement design temperature is not exceeded under field conditions.

2.4 Temperature Model Calibration

The overall temperature prediction model was calibrated based on field data collected from seven CRC construction sites visited during this study. Concrete temperatures measured in the field were compared to the temperatures predicted with the temperature model. Based on the average r^2 values, it may be concluded that in 27% of the case. This indicates that 78% of the measured in-place concrete temperatures can be explainable by the temperature prediction model. The error obtained between the measured and predicted maximum in-place concrete temperature ranged between -4.6% and 3.4%.

The obtained r^2 values are in general high for the prediction of in-place behavior. This indicates that the majority of the experimental data are explained by the developed model. Based on this calibration and the temperature predictions, it may be concluded that the temperature prediction model is able to produce accurate predictions of early-age concrete temperatures in concrete paving applications.

The program was successfully calibrated for the variables that may have a significant impact on the in-place concrete temperature. It may be concluded that the proposed temperature prediction model could be used as a tool (design aid) to evaluate the effect of different cement contents, cement composition, water-cement ratio, cement fineness, mineral admixtures, initial concrete temperature at placement, environmental conditions, curing method, subbase temperature, pavement thickness, and time of placement. This calibration model will allow the designer/contractor to evaluate, in a short time frame, the effect of the different options on the predicted in-place concrete temperature development.

2.5 Initial and Final Set of Concrete

Final setting of concrete relates to the point where stresses and stiffness start to develop in freshly placed concrete. With knowledge of the time to initial set, contractors will be able plan measures to finish and texture the concrete pavement in time to prevent setting occurring before these activities. In this study, experimental work was performed under laboratory and field conditions to determine the effect of temperature, different cements, and mineral admixtures on the initial and final times.

ASTM C 403 (1998) setting data were collected under field and laboratory conditions for concrete mixtures containing different cements, fly ash types, and GGBF slag. The water-cementitious materials ratio of the mixtures varied between 0.39 and 0.54, and the cement factor varied between 5.0 and 6.5 sacks of cement. It is found the setting of concrete in general occurs when a specific amount of hydration products have been formed. These findings are in agreement with those reported by Byfors (1980), Chen and Odler (1992), and more recently Pinto and Hover (1999).

The formulation shown in Equation 2.9 was used to incorporate the effect of the water-cementitious materials ratio into the degree of hydration at initial and final set.

$$\alpha_{cr} = k_s (w/c) \quad (2.9)$$

where

α_{cr} = critical degree of hydration,

k_s = constant that varies between 0.4 and 0.46, and

w/c = water-cement ratio

This is necessary because a higher water-cement ratio indicates a greater distance between cement particles, which will in turn require a higher degree of hydration before stiffening of the mixture occurs. The ratio between the critical degree of hydration at setting and the water-cementitious materials ratio for initial and final set was investigated. The results reveal that for most mixtures, the ratio appears constant. However, when GGBF slag is used, setting occurs at an earlier degree of hydration. It is for this reason recommended that the interaction between setting and hydration of GGBF slag be further investigated.

It is recommended to use the following formulations to estimate the degree of hydration at initial and final set:

$$\text{ASTM C 403 initial set: } \alpha_i = 0.15(w/cm) \quad (2.10)$$

$$\text{ASTM C 403 initial set: } \alpha_f = 0.26(w/cm) \quad (2.11)$$

Where

α_i = degree of hydration at initial set,

α_f = degree of hydration at final set, and
 w/cm = water- cementitious materials ratio.

The test results obtained through penetration resistance testing (ASTM C 403) provide useful data that can be used to characterize the setting of concrete at early-ages. It is recommended to compare set times in terms of equivalent ages. For this reason, it is further recommended to measure the temperature development in the mortar specimens used in the ASTM C 403 test.

2.6 Summary

The study developed mitigation techniques to control the in-place temperature development of early-age concrete. Longer lasting PCC pavements will be produced if the assumptions made during design are achieved in the field. This study proposes a method to integrate the design assumptions to the construction process by means of an end-result temperature control specification.

A general hydration model for cementitious materials and a model to predict the temperature gain in hardening concrete was developed and calibrated. The temperature prediction model was calibrated for field conditions with data collected from seven concrete paving projects. The model accounts for different pavement thicknesses, mixture proportions, cement chemical composition, cement fineness, amount of cement, mineral admixtures, material types, climatic conditions, and different construction scenarios. The temperature prediction model will enable the development of performance-based specifications to guard against premature concrete failures. This model will further provide the designer, contractor, and specification developer with the means to evaluate and quantify the effect of most of the various complex interactions that affect the concrete temperature development during early-ages.

A model to predict initial and final setting of hardening concrete was presented, and calibrated, with data collected under laboratory and field conditions. The effects of concrete temperature, different cements, and mineral admixtures on the initial and final times were characterized.

Chapter 3. Moisture Related Cracking Effect on Concrete Pavement

3.1 Overview

Hydrating concrete pavement is typically subjected to both moisture and temperature-induced stresses that drive cracking mechanisms at early concrete ages. Undesirable cracking resulting from these mechanisms plays a key role in both short- and long-term performance of most concrete pavement systems. Short-term performance is heavily dependent upon curing quality and construction weather, while curling and warping behavior can have both short- and long-term consequences. The focus of this chapter is primarily on the short-term perspective and how moisture profile and curing quality effects are involved in warping behavior and, ultimately, delamination cracking and spalling distress.

3.2 Moisture-related Strength Factors in Concrete Pavements

It is suggested that the linear relationship between the double natural logarithm of relative strength and the natural logarithm of the maturity is independent of curing temperature. Once the strength-maturity relationship is obtained for a given mixture design, this relationship can be used to find the opening maturity under any curing temperature. To consider the effect of moisture on the strength-maturity relationship, the Nurse-Saul maturity model was modified by including a moisture modification factor, as suggested by Bažant.

A moisture modification factor shown in Equation 3.1 was originally modeled for numerical computation of moisture effect on equivalent curing time (Bažant, 1969) on the basis of the observation of concrete moisture (Powers, 1947).

$$\beta_H = [1 + (7.5 - 7.5H)^4]^{-1} \quad (3.1)$$

where

β_H = moisture modification factor, and
 H = humidity of concrete.

The value of the moisture modification factor decreases as the relative humidity of the concrete decreases. The moisture modification factor represents the influence of moisture upon the rate of hydration reaction. Therefore, strength of concrete at a level of moisture can be adjusted by use of the moisture modification factor. It is suggested that the temperature-based maturity may be adjusted by incorporating the moisture modification factor into the Nurse-Saul maturity function as:

$$M_H = \beta_H \cdot \sum_0^t (T - T_0) \Delta t = \frac{\sum_0^t (T - T_0) \Delta t}{1 + (7.5 - 7.5H)^4} \quad (3.2)$$

Where

M_H = maturity at age t (°C-hrs),
 β_H = moisture modification factor,

T = average temperature of the concrete during time interval Δt (°C), and
 T_0 = datum temperature (°C).

The moisture modification factor originally was developed based on the observation that hydration stopped when the relative humidity of the drying concrete decreased to approximately 80%. However, concrete strength steadily increased below 80% of relative humidity and, as a result, the moisture modification factor was modified. Moisture-modified maturity is reformulated by using the corrected moisture modification factor.

$$M_H' = \beta_H' \cdot \sum_0^t (T - T_0) \Delta t = \frac{\sum_0^t (T - T_0) \Delta t}{1 + (5 - 5H)} \quad (3.3)$$

The improved linear logarithmic relationship between relative strength and maturity was made by using the corrected moisture modification factor. To consider the moisture variation due to environmental conditions in the field, a cumulative moisture modification factor that utilizes moisture history of concrete needs to be incorporated.

Temperature distributions of the concrete pavement are estimated by analyzing the transient heat transfer between the concrete and the surrounding condition as represented by the boundary value equations where the effects of environmental factors such as air temperature, wind velocity, solar radiation, and heat of vaporization are accounted for. The heat of hydration also must be considered to accurately estimate temperature distributions of the early-age concrete pavement. The hydration process generates internal heat, which influences the rate of chemical reactions of the cementitious materials and water while the environmental conditions influence concrete temperature and moisture conditions at the surface.

3.3 Evaporation Modeling

Early age moisture loss from the surface of a concrete pavement may induce undesirable effects that decrease long-term performance. Early-aged detrimental behaviors such as slab curling, warping, delamination, and even plastic shrinkage cracking are affected by the amount of evaporation and the effectiveness of the curing medium. The rate of evaporation is a key item relative to monitoring the quality of the curing. However, most approaches for this are largely empirical and are only useful under laboratory conditions. The effective curing thickness concept is introduced as a method to evaluate the curing effectiveness of a curing method. The surface relative humidity has the biggest influence on both the effective curing thickness and the rate of evaporation. Prediction of the evaporation rate of concrete depends on the surface relative humidity and is important for evaluation of the method of curing. Existing evaporation models, including the American Concrete Institute (ACI) nomograph, were evaluated relative to their capability to predict the evaporation from the curing concrete.

A test methodology was developed to evaluate curing methods for concrete pavement. Effective curing thickness is suggested as a parameter to evaluate or assess the quality of curing concrete. Maintaining higher levels of surface relative humidity is important for better curing quality. The curing condition was influenced by wind speed significantly, and minimization of wind effects is an important factor for high curing quality. None of the existing evaporation models were suitable to predict the evaporation of concrete after bleeding because they were

developed based on an evaporation condition that is consistent with a continuous layer of water on the concrete surface. A modified version of Penman's model is described in Equation 3.4 based on concrete's drying characteristics after bleeding.

$$E = \delta \frac{Q_s}{H_v} + J \quad (3.4)$$

where

E = rate of evaporation from concrete due to both net radiation and aerodynamic effects (kg/m²/hr),

τ^m = calibration factor for moisture condition of concrete surface,

Q_s = solar radiation absorption through electromagnetic waves (kg/m/hr),

$$= \alpha \left[I_d \sin \theta + I_i \left(\frac{1 + \cos \gamma}{2} \right) \right] \text{ (Branco, 1992),}$$

α = surface heat absorptivity of concrete (= 0.6) (Chapman, 1982),

I_d = direct solar radiation (kg/m/hr),

I_i = indirect solar radiation (kg/m/hr),

θ = incidence angle of solar radiation against the slab surface (degree),

γ = inclination angle of slab surface (degree),

H_v = heat of vaporization (heat removed from water on the surface of the concrete slab being vaporized),

J = rate of evaporation from concrete due to convective heat transfer, irradiation, and aerodynamic effects (kg/m²/hr)

The largest difference from the original Penman's model was reflected in the drying characteristics of the concrete in predicting evaporation. Also, the surface moisture emissivity was characterized by a series of experiments. The surface moisture emissivity was found to be a function of effective curing thickness and wind speed. Another difference involves the adjustment of the solar radiation effect by the effective curing thickness. The modified Penman's model will allow for improved prediction of the amount of evaporation at a concrete pavement and evaluation of the method of curing.

3.4 Evaporation-induced Cracking

Shear stress (or delamination stress) can be determined based on slab curling and warping behavior. Slab warping (mainly driven by differential drying shrinkage) can occur in two stages as denoted by Tang et al., (1993) delineated by separation of the slab corner from contact (i.e., liftoff) with the subgrade versus where the slab is in contact with the subgrade (i.e., zero liftoff). A set of functions developed on this basis was formulated to determine either edge or corner deflection due to curling and warping. In assuming the following model form for deformation at a slab corner, a form similar to that used by Tang et al. (1993) was adopted as:

$$w = \frac{(A_1 \cos x + A_2 \sin x)(B_1 \cos y \cosh y + B_2 \sin y \sinh y)}{e^x} \quad (3.5)$$

where

$$y = Y/l,$$

$$x = X/l,$$

$$Y = \text{distance from slab corner along the transverse joint,}$$

$$X = \text{distance from slab corner along the longitudinal joint, and}$$

$$A_i, B_i = \text{function coefficients}$$

Medium-thick plate theory provided the basis for several boundary conditions that were considered in the development of the coefficient equations.

3.4.1 Sensitivity of Moisture to Delamination Stress

A two-dimensional finite element program, TMAC², was developed to predict the moisture and temperature profiles of a concrete pavement in specified environmental conditions and simultaneously account for these important factors and concrete pavement performance. Darcy's Law was used as a governing equation of moisture diffusion in TMAC² to model the moisture profiles. The finite element mesh of TMAC² has a total of 120 rectangular elements (5 columns \times 24 rows) with 539 nodal points (9 nodal points per each element). TMAC² simultaneously models the moisture and temperature of a concrete pavement in specified environmental conditions. Many other capabilities such as prediction of strength, elastic modulus, and tensile creep development, and design of mixture proportion have been incorporated into the software.

A limited sensitivity study was conducted using analysis from the TMAC² program and the delamination model. The sensitivity of moisture profiles to delamination stress was examined in two parts—one part by fixing key parameters at reasonable and typical levels. Temperature and moisture-related parameters were varied over a selected range in the analysis to examine their effect on the delamination stress development. The parameters that were varied were:

- Equivalent Linear Humidity Difference Coefficient
- Equivalent Linear Temperature Difference
- Ultimate Concrete Shrinkage
- Coefficient of Thermal Expansion

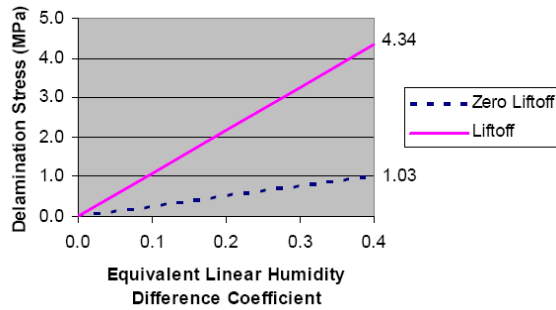
Table 3.1: Typical values of parameters of delamination model

Parameters	Value
Slab thickness	10 in.
Slab width	12 ft.
Concrete elastic modulus	3000 ksi
Concrete Poisson ratio	0.15
Modulus of subgrade reaction	100 pci
Delamination depth	1 in.

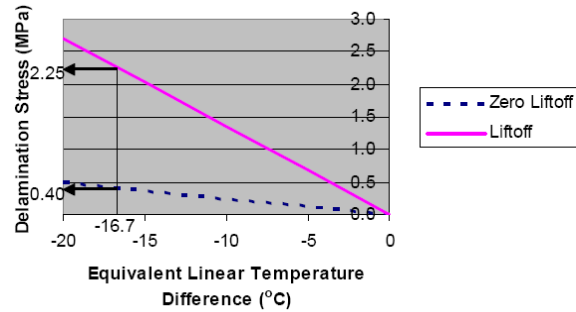
Delamination stress is affected by moisture profiles in concrete as shown in Figure 3.1 (a). The delamination stress increases with an increase of the equivalent linear humidity difference coefficient (Vepakomma et al., 2002). Because a larger humidity difference coefficient is

calculated by larger changes in concrete moisture profiles, the potential for delamination will be greater. Delamination stress under liftoff conditions is much stronger than for zero liftoff conditions. Sensitivity of temperature difference on the delamination stress also was examined, as shown in Figure 3.1 (b), and compared to its sensitivity to moisture difference.

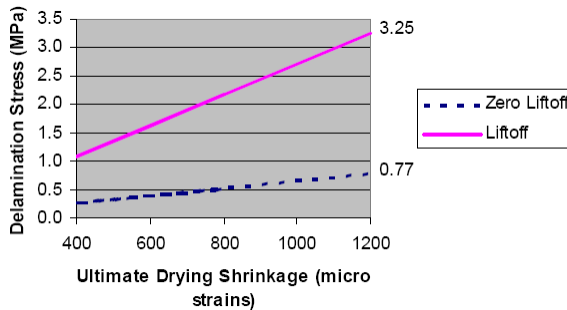
For this analysis, the maximum temperature gradient has been assumed to be about 3°F/inch during daytime and about 1 °F/inch during nighttime. Moisture effect on the delamination stress development is much larger than the temperature effect. Ultimate drying shrinkage of concrete and to some extent the *coefficient of thermal expansion* (CoTE) have effects on the delamination stress as shown in Figure 3.1 (c) and (d), respectively, although these effects were less than moisture or temperature difference effects. The minimum and maximum ultimate shrinkage strain and CoTE values were assumed to be 400 and 1200 micro-strains, and 6 and 14 micro-strains/°C, respectively. Slab width, subgrade reaction modulus, and ratio of delamination depth to slab thickness also have an effect on the magnitude of delamination stress.



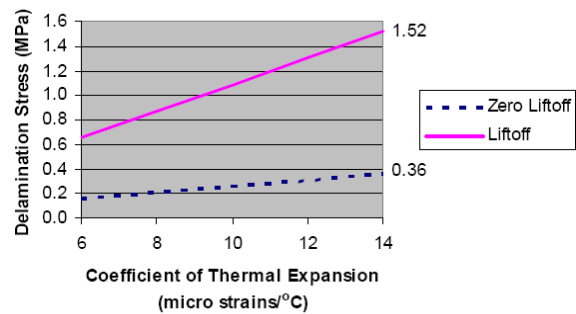
(a) Humidity difference



(b) Temperature difference



(c) Ultimate shrinkage



(d) Thermal expansion

Figure 3.1: Sensitivity study for delamination stress

3.4.2 Wind Speed, Curing Quality, and Aggregate Bond

The second part of this analysis focuses on other key factors affecting the formation of delamination of wind speed, curing quality, and aggregate bond strength. The evaporation depends largely on the speed of the wind over the evaporating surface. Wind replaces the air over a hydrating concrete surface that tends to become gradually saturated with water vapor. If

this air is not continuously replaced with drier air, the driving force for evaporation decreases. As the surface of the concrete dries, a moisture gradient develops typically in the top 3 inches of the concrete, which exposes concrete pavement to delamination stress. Analysis of wind effect on moisture distribution was conducted by use of the TMAC² program. High wind speed of 15 mph and low wind speed of 5 mph were selected in the analysis and other inputs were consistent with the field data collected from the US 59 test section. For a 5-mph wind speed condition, there is no obvious crossover between strength and delamination over time as shown in Figure 3.2. For a 15-mph wind condition, however, the strength is exceeded at the time of 10 hours after placement.

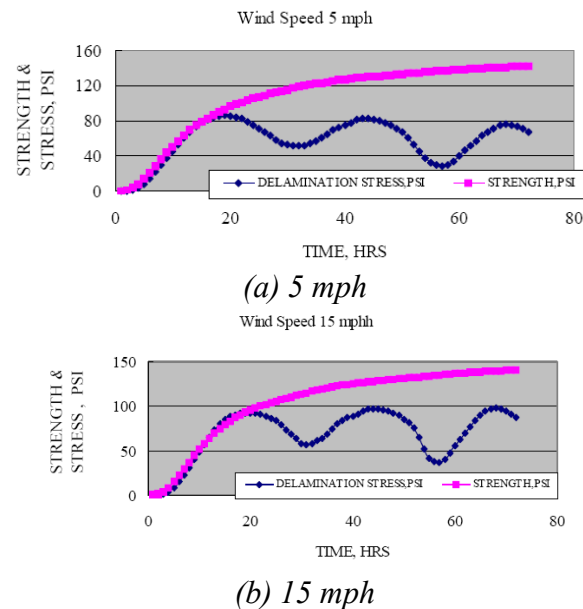


Figure 3.2: Effect of wind speed on delamination stress

Quality curing can effectively prevent moisture from evaporating from inside the concrete to the ambient air above it. The curing media works to seal the moisture below the concrete pavement surface. Effective curing thickness (ECT) is a useful index to evaluate curing quality. Laboratory testing data indicated that surface humidity, which is an important boundary condition for moisture analysis, is a function of ambient relative humidity, wind speed, and effective curing thickness.

A similar TMAC² analysis as shown in Figure 3.2 was carried out again to evaluate the impact of curing quality on delamination. An average of 1 inch and 2 inch effective thickness was used in the TMAC² analysis, and a wind speed of 15 mph was used to illustrate the effects of these parameters. For a 2-inch ECT, there was no obvious crossover between strength and the delamination stress. However, for a 1-inch ECT, the shear strength of the concrete was exceeded at the time of 10 hours after placement. This result indicates proper curing application can reduce the probability of delamination. It is clear that low bond strength aggregates and curing that averages an ECT of 1 inch or less will experience a high probability of delamination, which will translate into a high percentage of pavements suffering spall damage. Coarse aggregates manifesting a higher bond strength experience a lower probability of delamination but not if the

wind speed during placement is too high. Prior to discussion of the specification for curing effectiveness, some explanation of the aggregate bond strength is presented.

3.5 Summary

Hydrating concrete pavement is typically subjected to both moisture and temperature-induced stresses that drive cracking mechanisms at early concrete ages. Undesirable cracking resulting from these mechanisms plays a key role in both short- and long-term performance of most concrete pavement systems. Short-term performance is heavily dependent upon curing quality and construction weather while curling and warping behavior can have both short- and long-term consequences. The focus of this chapter is primarily on the short-term perspective and how moisture profile and curing quality effects are involved in warping behavior and ultimately delamination cracking and spalling distress.

Based on this perspective, mathematical models were developed for the calculation of moisture and temperature profiles to help investigate the effect of different combinations of climate, construction, and materials on the development of the moisture and temperature profiles and their subsequent effects on early-aged cracking. These models appear as nonlinear time-dependent partial differential equations and are solved by the finite element method simultaneously that involves both backward and forward calculation. Using measured test data, moisture diffusivity and thermal conductivity were back-calculated to facilitate accurate modeling of moisture and temperature flows in hardening concrete. On the whole, the calculated moisture and temperature profiles using the moisture diffusivity and thermal conductivity models corresponded to the measured data.

Spalling typically occurs at random cracks and occasionally at joints subjected to high delamination stresses during and shortly after construction. The incidence of this distress type is strongly correlated to pre-existing horizontal delaminations that occur within 1 in. of the pavement surface and can later grow into a spall due to a variety of causes. The cause of the shallow, horizontal delaminations that occur within the top 1 in. of the pavement surface is primarily from early-age nonlinear shrinkage strains in addition to temperature variations through slab depth. Thus, the factors of the most importance are those related to the effectiveness of the curing medium in minimizing moisture loss during the hydration of the concrete and the bond strength between the aggregate and the paste. By increasing the effectiveness of the curing system, moisture gradients near the surface are substantially reduced and delamination stress minimized.

Chapter 4. Sensitivity Analysis of CRCP Computer Programs

4.1 Overview

4.1.1 Background

The first mechanistic model, CRCP-1, was developed in the mid-1970s under a study sponsored by the National Cooperative Highway Research Program (McCullough et al., 1975). CRCP-2 was developed in 1977 by extending the original steel stress model to cover situations where development length under the influence of high frictional resistance might exceed half the crack spacing (Ma and McCullough, 1975). In 1991, Won et al. developed an improvement to the CRCP program, CRCP-5, which simulates material variance to concrete tensile strength and includes fatigue failure models (Won et al., 1991). The normalized curing curves were determined for different coarse aggregates commonly used in Texas pavements (Dossey and McCullough, 1991), and these curves and the calibrated failure prediction model were included in CRCP-7 (Suh et al., 1992). In 1995, previous versions of the CRCP programs were integrated into one program, CRCP-8, with simplification of the user input process (Won et al., 1995).

Although CRCP-8 has permitted pavement engineers to develop and evaluate designs of CRCP, there are some limitations due to the simplified assumptions in the one-dimensional analysis. In 1996, a research project was conducted to expand the ability of the mechanistic model by incorporating the variations in temperature and moisture changes through the depth of concrete slab. As a result of the project, a two-dimensional finite element model of CRCP was developed (Kim et al., 1997; Kim et al., 1998). In 1998, the Texas Department of Transportation (TxDOT) decided to extend the project to complete the development of a new mechanistic model, CRCP-9. CRCP-9 uses two-dimensional finite element theories to reduce the cost of computation, but to increase the accuracy of the 2-D model, three-dimensional analyses were also performed, and the differences between 2-D and 3-D analyses results were investigated (Kim et al., 2000). In CRCP-9, the external wheel load stresses are calculated considering a static single wheel load (Kim et al., 2001). The current program in the development sequence is the CRCP-10 Program.

4.1.2 Objectives

The objective of this report is to document the results of the initial steps in the process of maximizing the accuracy and reliability of the CRCP-10 program. The secondary objectives are as follows:

- Compare the output of the CRCP-8 and CRCP-10 programs using identical input insofar as possible that reflects the range of variables that may be experienced. These results are then used to apply a “test of reasonableness to the output values.”
- Once the CRCP-10 output is deemed satisfactory, the input variables will be ranked as to their effect on the sensitivity of the output.

4.1.3 Approach

To maximize the accuracy and reliability of the program, a calibration and validation with field data needed to be performed. Because CRCP-8 has been calibrated previously, and validation studies have shown very close agreement with field data, the results from CRCP-10 were compared with those from CRCP-8 before performing the calibration with field data. The process of maximizing the accuracy and reliability of CRCP-10 is a three-step process as follows:

- The first step is to evaluate the viability of the program by comparing it to the CRCP-8 program and to apply a “test of reasonableness” to the output for realistic input values.
- The second step is to rank the input variables as to their significance on affecting the output.
- The third step is to calibrate if needed and to validate using existing data or from test sections constructed with a range of the significant variables.

The material presented herein pertains to the first two steps. Thus, after the results are evaluated, the third step will be organized, developed, and then used for calibration and/or validation.

4.2 Input Variables

The choice of levels of factors to be used in an experiment depends upon the nature of the experimental yields and upon the objectives of the experiment. A three-level experiment was established here; each input variable was given low, medium, and high values, based on engineering judgment and literature reviews (Won et al., 1991; Dossey and McCullough, 1991; Suh et al., 1992; McCullough et al., 1999; Chiang et al., 1975). Medium levels are those that might be met in practice under average design conditions. A low level is a practical value at the lower extreme with respect to the medium level, while a high level is a practical value at the upper extreme.

The low, medium, and high values of each variable selected in this study are listed in Table 4.1. Medium levels are what might be met in practice under average design conditions. A low level is a practical value at the lower extreme with respect to the medium level, while a high level is a practical value at the upper extreme. Because there are different input variables in some cases between CRCP-8 and CRCP-10, Table 4.1 shows both input parameters.

4.3 Sensitivity Analysis Results

The sensitivity analysis of the design variables has been conducted to obtain the effect of each variable on the CRCP behavior, to find the relative importance of each variable, and to compare the results between CRCP-8 and CRCP-10. In the sensitivity analysis, one variable is selected and changes within the practical range while the other variables remain at their medium values, and the analysis results such as mean crack spacing, crack width, and steel stress at crack, are obtained. In the following sections, these results are first discussed in general terms, and then in terms of specific inputs.

Table 4.1: Summary of low, medium, and high values of each variable

CRCP-10	Low	Medium	High	CRCP-8
Concrete Properties				Concrete Properties
Pavement Thickness (in.)	6	12	15	Pavement Thickness (in.)
Poisson's Ratio of Concrete	0.15	0.15	0.15	
Specific Weight of Concrete (pcf)	100	145	145	
Coefficient of Variation for Concrete Tensile Strength (%)	10	15	20	Coefficient of Variation for Concrete Tensile Strength (%)
Coarse Aggregate Type				Coarse Aggregate Type
COTE (microstrain/F)	3	5	8	COTE (microstrain/F)
Elastic Modulus at 28 Days (psi)	3,640,000	4,220,000	4,930,000	Elastic Modulus at 28 Days (psi)
Tensile Strength at 28 Days (psi)	430	530	650	Tensile Strength at 28 Days (psi)
Drying Shrinkage at 256 Days	0.000342	0.000394	0.000461	Drying Shrinkage at 28 Days
Steel Properties				Steel Reinforcement Properties
Elastic Modulus of Steel Bar (psi)	29,000,000	29,000,000	29,000,000	Elastic Modulus (psi)
Steel Bar Diameter (in.)	0.625(No.5)	0.75(No.6)	0.875(No.7)	Steel Bar Diameter (in.)
Thermal Coefficient (microstrain/F)	5	5	5	Thermal Coefficient (microstrain/F)
Specific Weight of Steel (pcf)	490	490	490	
Percent Reinforcement (Steel Ratio) (%)	0.4	0.6	0.8	Percent Reinforcement (Steel Ratio) (%)
Slab/Subbase Resistance				
Vertical Stiffness of Subgrade (psi/in.)	300	700	1,200	
Subbase Type	Asphalt	Flexible	Cement	Slab-Base Friction Curve Type
Horizontal Stiffness/Unit Area (psi/in.)	55.9	145.5	15,400	
External Wheel Loads				External Load
Days after Concrete Sets before Wheel Load Applied	3	7	28	Days after Concrete Sets before Wheel Load Applied
Static Single Wheel Load				Static Single Wheel Load
Wheel Load (lbs.)	6,000	9,000	12,000	Wheel Load (lbs.)
Wheel Base Radius (in.)	6	6	6	Wheel Base Radius (in.)
Climatic Loads				Environmental Load
Zero-Stress Temperature (F)	60	90	125	Zero-Stress Temperature (F)
Min. Temperature at First Day after Placement (F)	50	60	70	Minimum Temperature (F)
Advanced Inputs				
Punchout Prediction Parameters				Punchout Prediction Parameters
Reliability (%)	50	75	95	Reliability (%)

4.3.2 General Observations

The analysis results point to the following observations:

- The crack spacing, crack width, and steel stress show similar trends in the results, but the crack spacing is more affected by changes in values of the design variables than the crack width and steel stress.
- The variables that make the crack spacing larger as they increase are
 - Pavement thickness
 - Tensile strength of concrete
 - Steel bar diameter
 - Minimum temperature at first day after placement
- The variables that make the crack spacing smaller as they increase are
 - Coefficient of variation for concrete tensile strength
 - Coefficient of thermal expansion of concrete
 - Percent reinforcement
 - Horizontal stiffness between concrete slab and subbase
 - Zero-stress temperature
- The most sensitive variables to the CRCP behavior are
 - Coefficient of thermal expansion of concrete
 - Zero-stress temperature
- The moderately sensitive variables to the CRCP behavior are
 - Pavement thickness
 - Coefficient of variation for concrete tensile strength
 - Tensile strength of concrete
 - Percent reinforcement
 - Horizontal stiffness between concrete slab and subbase
 - Minimum temperature at first day after placement
- The least sensitive variables to the CRCP behavior are
 - Steel bar diameter
 - Vertical stiffness of underlying layers
- Static single-wheel load and dynamic tandem-axle load have a significant influence on the pavement behavior, thus, the accurate prediction of wheel load is necessary during the design stage.
- The results from the CRCP-8 and CRCP-10 computer programs are generally in agreement. However, there is a large difference in the steel stresses between the two programs.

4.3.3 Concrete Properties

The sensitivity study of concrete material properties such as pavement thickness, coefficient of variation for concrete tensile strength, coefficient of thermal expansion, and tensile strength has been performed.

Three pavement thicknesses of 6, 12, and 15 inches are selected as low, medium, and high values, respectively. The crack spacing increases as the pavement thickness increases, but when the pavement thickness is over 10 inches for CRCP-10 and over 12 inches for CRCP- 8, the pavement thickness does not affect the crack spacing. The same result can be observed for the crack width and steel stress.

For coefficient of variation for concrete tensile strength, three values of 10%, 15%, and 20% are considered. With an increase in the coefficient of variation for concrete tensile strength, the crack spacing, crack width, and steel stress decrease. The decrease in the crack spacing is larger than that in the crack width and steel stress.

Three basic levels of coefficient of thermal expansion are selected to be 3, 5, and 8 microstrain/°F. The crack spacing decreases as the coefficient of thermal expansion of concrete increases. The rate of the decrease in the crack spacing is higher when the coefficient of thermal expansion is around the low values. The crack width and steel stress, however, are not significantly affected by the change of the coefficient of thermal expansion.

Three tensile strength values of 430, 530, and 650 psi are used to investigate the influence of concrete strength on the pavement behavior. The crack spacing, crack width, and steel stress increase with increasing the concrete tensile strength. The crack spacing is more affected by the change in tensile strength than the crack width and steel stress.

4.3.4 Steel Properties

Three different bar diameters were selected to investigate its effect on the pavement behavior. Those are 0.65 (No.5), 0.75 (No.6), and 0.875 (No.7) inches. The crack spacing increases very slightly with increasing the steel bar diameter. The crack width and steel stress are not affected as much by the steel bar diameter.

For the sensitivity of the percent reinforcement, three levels were selected to be 0.4%, 0.6%, and 0.8%. The mean crack spacing, crack width, and steel stress decrease as the percent reinforcement increases. As the amount of the steel reinforcement increases, the restraint to resist the concrete contraction due to the climatic loads, such as changes in temperature and drying shrinkage, becomes larger and the concrete stress increases. This causes more cracks and smaller crack spacings. The crack spacing can be up to 30% larger and 20% smaller than the typical crack spacing within the practical range of the percent reinforcement. It is noted that the sensitivity of the crack width and steel stress is very similar to that of the crack spacing in this case.

4.3.5 Slab/Subbase Resistance

The sensitivity of other design variables, including vertical stiffness of underlying layers and horizontal stiffness at the interface between the bottom of concrete slab and subbase, have been studied. Three levels of vertical stiffness were selected: 300, 700, and 1,200 pci. The vertical stiffness of underlying layers does not affect the analysis results. This means that the vertical stiffness of underlying layers is not a sensitive design variable when the other variables are at their typical values.

Asphalt-stabilized (56 pci), flexible (145.5 pci), and cement-stabilized (15,400 pci) subbase types are selected to investigate the effect of the horizontal bond stiffness at the interface between concrete slab and subbase. The crack spacing becomes smaller as the horizontal bond stiffness increases. The crack width and steel stress also decrease with increasing the horizontal

bond stiffness. Because the frictional bond stiffness is directly related to the subbase type, the selection of the subbase type affects the CRCP behavior significantly.

4.3.6 External Wheel Loads

The effects of the static single-wheel load and dynamic tandem-axle load have been studied. In this study, three different external wheel loads were selected: 6,000, 9,000, and 12,000 pounds. If there is no wheel load and only the climatic loads are applied, the crack spacing is not affected by the pavement thickness if the percent reinforcement remains the same. As the wheel load increases, the crack spacing becomes clearly affected by the pavement thickness. With increasing the pavement thickness, the crack spacing becomes larger. However, if the pavement thickness is over a certain value, the crack spacing is no longer affected by the pavement thickness. The pavement thickness that makes no change in the crack spacing becomes larger as the wheel load increases.

The static tandem-axle loads yield slightly larger crack spacings than the static single-wheel load. For moving tandem-axle loads of constant amplitude, the crack spacing is not affected by the speed of vehicle. However, moving tandem-axle loads of varying amplitude yield smaller crack spacing than that caused by the static tandem-axle loads, when the pavement thickness is smaller than a certain value.

4.3.7 Climatic Loads

Three zero-stress temperatures of 60°F, 90°F, and 125°F are examined. The crack spacing decreases as the zero-stress temperature increases. Although the variation of crack spacing is drastically changed with increasing zero-stress temperature, the computed crack width and steel stress are not much affected by the zero-stress temperature.

To consider different situations of daily temperature change during the curing period, three different first day's minimum temperatures are selected: 50°F, 60°F, and 70°F. The minimum temperature at first day after placement also affects the crack spacing. The crack spacing increases with increasing the minimum temperature. The crack width and steel stress show the similar results, but the variations are smaller.

4.3.8 Summary of Sensitivity

Table 4.2 summarizes the sensitivity of the design variables considered in this study. If the analysis results are over 30% different from the result obtained with the medium input value, the results are highlighted. As indicated in Table 4.2, the zero-stress temperature and the coefficient of thermal expansion are the most sensitive design variables. The steel bar diameter and the vertical stiffness of underlying layers are not sensitive design variables, and the other design variables can be defined as moderately sensitive design variables.

The sensitivity of the design variables to the steel stress obtained from CRCP-8 and CRCP-10 is very similar. However, the absolute values of the steel stresses from the two programs show a large difference. Further studies, including field experiments, are needed to find the actual steel stresses.

Table 4.2: Sensitivity of design variables

Input Variables	Variations of Relative Values based on Medium Outputs				
	Results	CRCP-10		CRCP-8	
		Low (%)	High (%)	Low (%)	High (%)
Pavement Thickness (in.)	Crack Spacing (ft.)	-51.3	0	-65.9	0
	Crack Width (in.)	-34.7	-3.6	-58.9	0.8
	Steel Stress (ksi)	-31.9	0.9	-39.9	2.3
Coefficient of Variation for Concrete Tensile Strength (%)	Crack Spacing (ft.)	23.3	-19.6	50.0	-32.5
	Crack Width (in.)	9.3	-9.9	41.9	-29.4
	Steel Stress (ksi)	10.2	-10.7	17.0	-17.8
COTE (microstrain/F)	Crack Spacing (ft.)	76.2	-43.1	92.9	-43.7
	Crack Width (in.)	-13.6	8.4	-4.9	-0.8
	Steel Stress (ksi)	-3.0	-5.8	5.6	-14.5
Tensile Strength at 28 Days (psi)	Crack Spacing (ft.)	-27.4	32.2	-34.1	50.0
	Crack Width (in.)	-14.0	12.7	-31.7	42.6
	Steel Stress (ksi)	-15.1	13.8	-17.9	20.6
Steel Bar Diameter (in.)	Crack Spacing (ft.)	-7.5	2.8	-6.9	8.0
	Crack Width (in.)	-7.3	4.5	-8.3	9.1
	Steel Stress (ksi)	-0.7	-1.7	4.4	-4.6
Percent Reinforcement (Steel Ratio) (%)	Crack Spacing (ft.)	32.2	-22.9	68.8	-34.1
	Crack Width (in.)	32.9	-18.7	71.7	-34.3
	Steel Stress (ksi)	35.7	-20.4	30.1	-20.3
Vertical Stiffness of Subgrade (psi/in.)	Crack Spacing (ft.)	0	0	0	0
	Crack Width (in.)	0.4	-0.2	0	0
	Steel Stress (ksi)	0	0	0	0
Horizontal Stiffness	Crack Spacing (ft.)	0	-66.4	0	-56.5
	Crack Width (in.)	0	-39.7	0	-55.1
	Steel Stress (ksi)	0	-48.6	0	-33.1
Zero-stress Temperature (F)	Crack Spacing (ft.)	363.3	-56.5	124.9	-55.0
	Crack Width (in.)	-0.4	-7.1	-7.9	-23.8
	Steel Stress (ksi)	-1.1	-5.1	-1.2	-14.4
Min. Temperature at First Day after Placement	Crack Spacing (ft.)	-31.5	54.2	-27.0	28.5
	Crack Width (in.)	-16.5	18.8	-24.2	24.5
	Steel Stress (ksi)	-17.7	20.5	-14.6	9.8

4.4 Summary

The sensitivity analysis of the design variables has been performed using mechanistic models of CRCP to investigate the effects of the variables on the CRCP behavior, to determine the relative importance of each variable, and to compare the results from CRCP-8 and CRCP-10. The practical ranges of the variables have been selected, and the typical values of the variables have been determined. In the sensitivity analysis, one variable is selected and changes within the practical range while the other variables remain at their typical values, and the analysis results such as mean crack spacing, crack width, and steel stress at crack are obtained.

From this study, the sensitivity of each design variable to the CRCP behavior has been investigated. The relationships between the design variables and the CRCP behavior have also been obtained. Engineers should pay close attention to characterizing the sensitive design variables while using the CRCP program in design or evaluation. Because engineers have only limited resources and time to use in estimating a large number of design variables, the findings described in this report can be applied to aid in solving real problems more efficiently and accurately.

The performed study in this chapter leads to the following primary conclusions:

- The material presented in input variables for the sensitivity analysis demonstrate the viability of both the CRCP-8 and CRCP-10 programs.
- The comparisons between programs and with field data show that the predicted crack spacing and crack widths are similar and compare favorably with field data.
- The actual magnitude of the steel stress for the CRCP-10 is approximately 2/3 of the CRCP-8, but the trends of the relative stress magnitudes with the various input data are identical. The selection as to which program has the correct magnitude cannot be made due to unavailability of field adequate data.
- The most sensitive variable affecting the performance of a CRCP in the field is the zero-stress temperature as demonstrated by previous studies (Suh et al., 1992), and the comparison of outputs from the two programs as shown in Table 6.1, “Sensitivity of Design Variables.” Hence, the need for exercising specification and field control using the PavePro program are emphasized as a way to mitigate the occurrence of premature punchouts.
- The zero-stress temperature sensitivity is primarily related to the crack spacing, but the reduced sensitivity of the crack width and steel stress may be attributed to the fact that these behavior parameters are directly related to the crack spacing.
- The second most sensitive variable affecting CRCP performance is the concrete COTE value. The results, thus, re-emphasized the need for a viable concrete COTE test and a database of COTE values.

Chapter 5. The Effect of Early Opening to Traffic

5.1 Overview

Flexural fatigue failure induced by repeated traffic loads is one of the basic structural distresses that affect the performance of pavement systems. To quantify the life prediction of a rigid pavement system, an appropriate fatigue equation is required. The majority of previous research has been conducted under laboratory testing conditions using reduced-scale specimens such as concrete beams and small slabs due to time and cost limitations.

5.1.1 Objectives

This chapter proposed to evaluate the early opening criteria of PCC pavements to traffic such that these criteria become implemented into TxDOT opening criteria for concrete construction projects. The following list briefly itemizes the main objectives of this research program:

- 1) Establishment of the fatigue relationship of typical paving mixture with normal strength concrete from by laboratory flexural fatigue testing;
- 2) Verification of provided fatigue relationship from the laboratory testing by the comparison with the data from the super-accelerated full-scale slabs fatigue testing;
- 3) Development of mathematical model which can quantify the loss of life due to early opening based on the fatigue equations from experiments; and
- 4) Evaluation of the current specification requirements for implementation.

5.1.2 Approach and Scope

The work plan for this study consists of the following three tasks:

- 1) Laboratory testing program. To quantify the life prediction of a rigid pavement system, an appropriate fatigue equation is fundamentally required. A series of laboratory fatigue testing was performed on simply supported beams to develop appropriate fatigue relationships for typical, normal strength Texas paving concrete mixture designs;
- 2) Super-accelerated pavement testing on full-scale concrete slabs using the Stationary Dynamic Deflectometer (SDD). The purpose of this testing were: (1) to determine the fatigue resistance of full-scale concrete slabs in the field and (2) to compare these results with laboratory beam fatigue test results for a given concrete mixture design. A reasonable fatigue relationship between laboratory specimens and field slabs would help to solve the size effect problem. Another goal of this testing was to evaluate the feasibility of the super-accelerated pavement testing technique using the SDD for fatigue loading of full-scale rigid pavements in a real field setting. The establishment of a practicable accelerated pavement testing technique would help to solve the time limitation factor of fatigue testing on full-scale pavement systems;

- 3) Development of a numerical model to evaluate the loss of life of a normal strength concrete pavement when it is opened to traffic prior to the design strength.

5.2 Concrete Materials

The concrete mixture designs used in this research were typical concrete paving mixtures used in the state of Texas. The same constituent materials were used exclusively throughout the testing program, including both the laboratory beams and field slabs. The target third-point loading modulus of rupture for the mixture was 555 psi at 7 days and 720 psi at 28 days. To investigate the effect of coarse aggregate on the static and fatigue strengths, two commonly used coarse aggregates were selected: crushed limestone (LS) and siliceous river gravel (SRG). All aggregates were used in a saturated, surface-dry condition and stored at the desired temperature conditions to ensure temperature equilibrium. The concrete mixtures used in this study are summarized in Table 5.1.

Table 5.1: Mixture proportions

Material Constituent	Quantities per yd ³ of Concrete	
	LS	SRG
Water (gal / lbs)	24.75 / 207	24.75 / 207
Cement (Type I) (lbs)	362	362
Class C Fly Ash (lbs)	155	155
Coarse Aggregate (lbs)	1,745	1,875
Fine Aggregate (lbs)	1,335	1,300
Air Content (%)	5	5
Air Entraining Agent (fl. oz)	2	2
Retarder (fl. oz)	8	8
Water-Cementitious ratio	0.40	0.40

5.3 Laboratory Beam Fatigue Testing

To provide the comparable maximum applied stress to number of cycles to failure ($S-N$) relationships for the field slab fatigue testing, a series of static and constant-amplitude cyclic loading tests was completed before the field slab testing. Seventy-eight beams were tested under constant cyclic loading: 42 SRG beams and 36 LS beams. All laboratory beams and test cylinders were cast and cured under controlled conditions. To simulate the various field conditions, laboratory beam fatigue testing was conducted under three different curing and testing temperature conditions (50° F, 75° F and 100° F) and three different ages of first loading (3, 7 and 28 days).

5.3.1 Laboratory Specimens

The static and fatigue beams were 6 in. by 6 in. by 36 in., and tested under third-point loading configuration with a span length of 33 in. To investigate the mechanical properties of

mixtures, compressive, splitting tensile strengths and elastic moduli were measured using 4 in. by 8 in. cylinders at the ages of 1, 3, 7, 14 and 28 days.

5.3.2 Laboratory Fatigue Testing Procedures

The simply supported third-point loading configuration was used to characterize the flexural fatigue and static behavior. In all fatigue testing, a constant amplitude sinusoidal waveform loading was used. All fatigue beams were loaded at 300 cycles per minute (5 Hz) with no rest period. The ratio of minimum-to-maximum cyclic load (R) was maintained at a constant 0.1. Fatigue specimens were tested to failure or to two million cycles of loading. Beams that did not fail after two million cycles were tested statically, and data were excluded for the $S-N$ relationships.

5.3.3 Laboratory Fatigue Testing Results

The generalized laboratory fatigue testing results for each coarse aggregate type is illustrated in Figure 5.1. Using log-linear regression, the $S-N$ relationship for each coarse aggregate type is as follows:

$$\text{Log } N = -11.57S + 13.22 \quad (R^2 = 0.72) \quad \text{for SRG mixtures} \quad (5.1)$$

$$\text{Log } N = -16.29S + 17.33 \quad (R^2 = 0.78) \quad \text{for LS mixtures} \quad (5.2)$$

where

N = the number of load repetitions to failure

S = maximum stress level

A comparison between the LS and SRG mix indicates reasonable results. The LS mixtures showed slightly higher static strengths (flexural, splitting tensile and compressive strength) than SRG mixtures but lower elastic moduli. Except for the very high stress levels (>0.9), the LS mixtures generally had a higher fatigue resistance than SRG mixtures for a given stress level.

The fatigue behavior of concrete is highly influenced by the minimum-to-maximum stress ratio, R . A slight increase of R decreases the fatigue life of concrete significantly. Shi et al. (1993) proposed a concept of equivalent fatigue life (EN) to overcome this problem. The equivalent fatigue life (EN) defined as follows:

$$EN = N^{1-R} \quad (5.3)$$

where

EN = equivalent fatigue life,

N = number of cycles to failure,

R = applied minimum-to-maximum stress ratio.

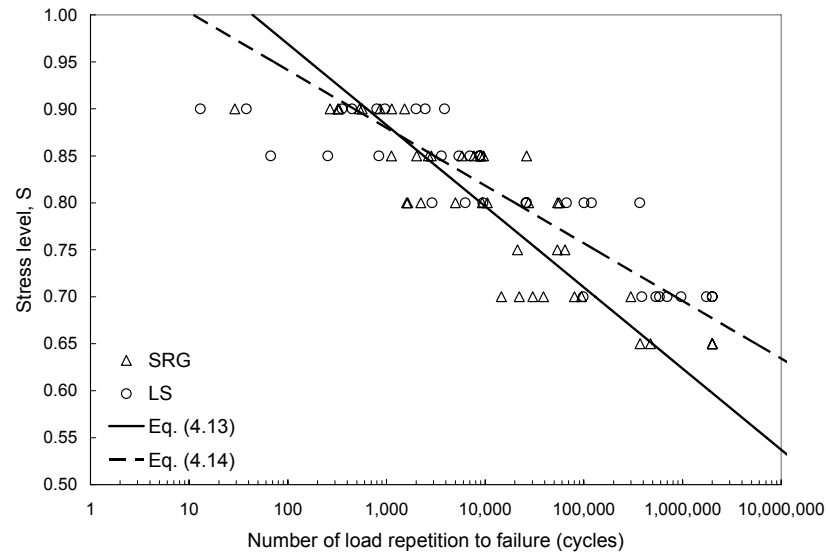
Beam fatigue life data (N) from this study can be converted to the equivalent fatigue life (EN) by applying Eq. (3). The equivalent $S-N$ relationship for each coarse aggregate type becomes:

$$\text{Log } EN = -9.33S + 10.98 \quad (R^2 = 0.72) \quad \text{for SRG mixtures} \quad (5.4)$$

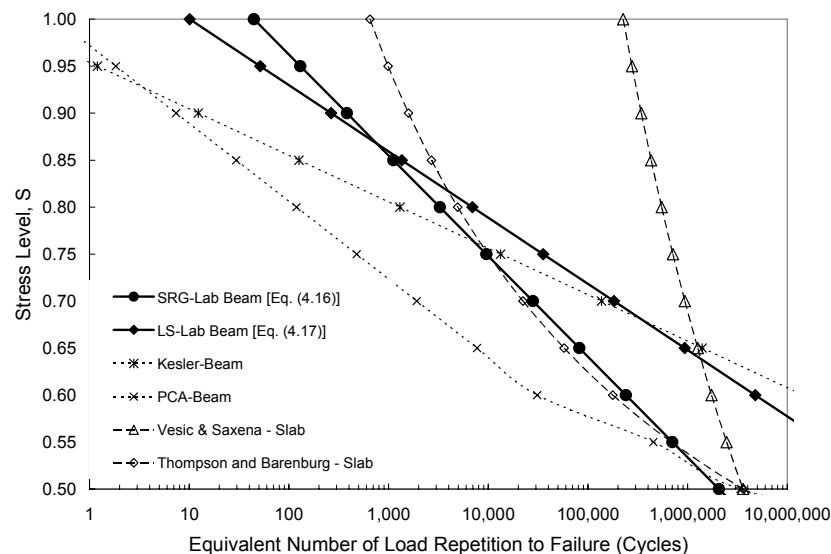
$$\text{Log } EN = -14.19S + 15.19 \quad (R^2 = 0.78) \quad \text{for LS mixtures} \quad (5.5)$$

Figure 5.1(b) shows the comparison of several existing fatigue curves and laboratory beam fatigue testing results. Kesler (1953) and PCA (1985) equations were developed based on

laboratory testing, while the other two curves were derived from the field slab testing. The Vesic and Saxena (1969) fatigue equation was derived from the AASHO Road Test data at a serviceability index equal to 2.5 as the function of the strength of concrete and the induced stress in the pavement. The Thompson and Barenberg (1992) curve was based on the results from Corps of Engineers' tests. The beam fatigue equations derived in this study shows less conservative N values compared to Kesler's (1953) results although their slopes are similar. The Thompson and Barenberg slab fatigue curve (1992) is very similar to SRG beam curve in the cases of relatively low stress levels.



(a) Laboratory beam fatigue testing results

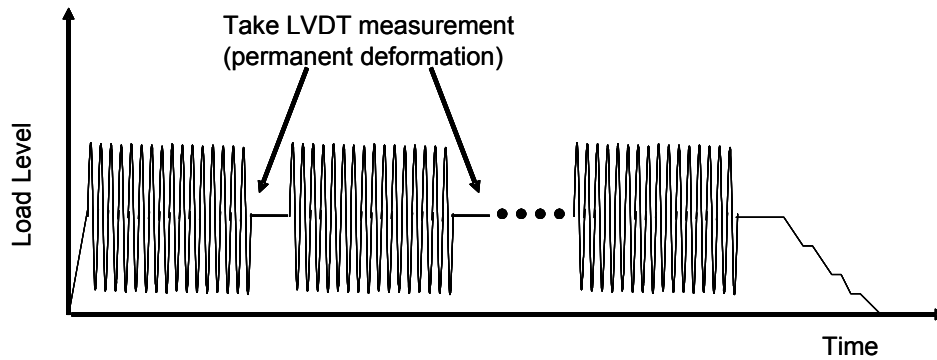


(b) Comparison of fatigue curves

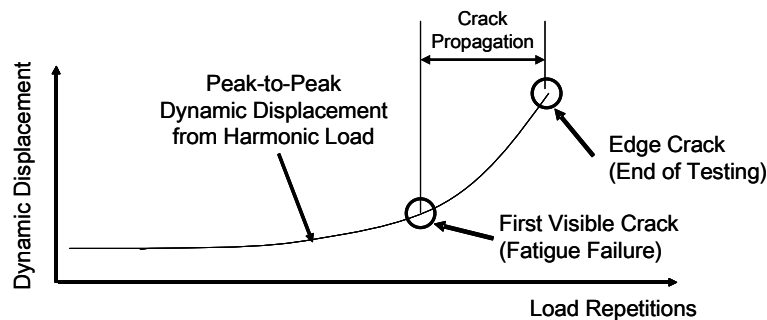
Figure 5.1: Summary of laboratory beam fatigue testing

5.4 Super-accelerated Slab Testing

The definition of super-accelerated pavement (SAP) testing is the application of one million load repetitions to a full-scale pavement system in a short time, on the order of 0.5 to 2 days, in nominal terms (Stokoe et. al, 2000). The test is conducted by applying cyclic loads generated by an external loading system through a loading frame placed on the pavement surface. The dynamic loads are created by the servo-hydraulic actuator that generates sinusoidal harmonic loads at a pre-selected frequency as illustrated in Figure 5.2(a). In the case of rigid pavements, the difference between the maximum and minimum displacements during dynamic loading was found to best represent the elastic response of the concrete slab by Roesler and Barenberg (1999, 1999). The variation of dynamic displacements during super-accelerated testing was found to be the main indicator to characterize the fatigue behavior of a rigid pavement system. In this study, fatigue failure of a full-scale slab was defined as the occurrence of the first visible crack. This occurrence generally accompanied abrupt changes in dynamic displacement. The conceptual diagram for the representation of pavement performance is illustrated in Figure 5.2(b). To investigate the propagation of cracks and stress redistribution, cyclic loading was applied until full depth cracking at the edges or joints of the pavement occurred.



(a) Sequence of load repetitions

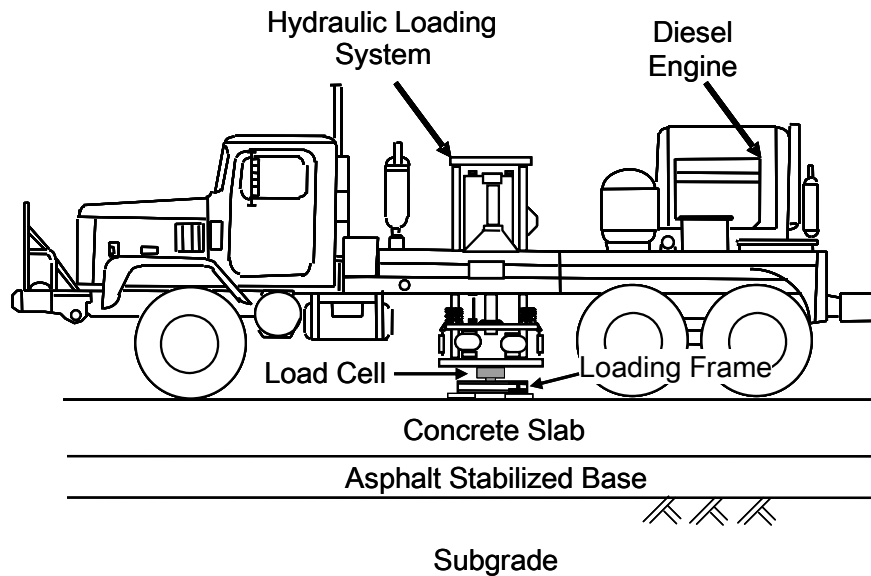


(b) Changes of dynamic displacement with increasing number of load repetitions

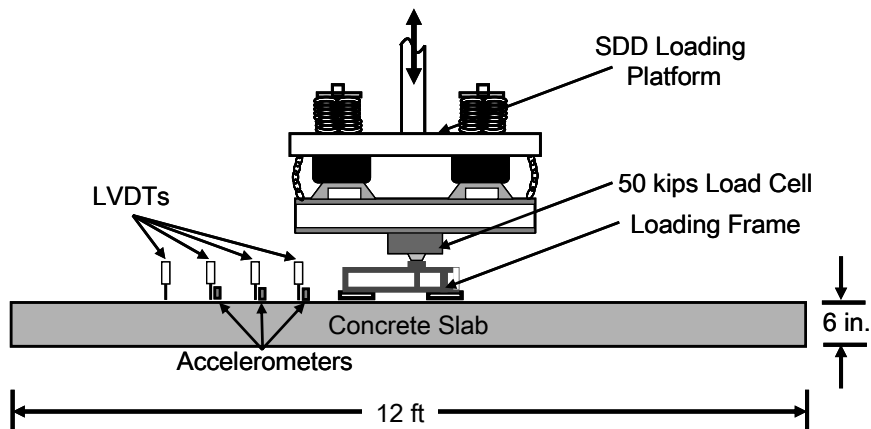
Figure 5.2: Illustrations of SDD testing method

5.4.1 Description of Stationary Dynamic Deflectometer (SDD)

Researchers at the University of Texas at Austin first developed the Rolling Dynamic Deflectometer (RDD) in the early 1990's (Bay et al., 1995; Bay et al., 1999). In the stationary mode, the device becomes a Stationary Dynamic Deflectometer (SDD). The SDD is a mobile accelerated pavement testing device, which can apply sinusoidal loads at a range of load levels and load frequencies. A diagram of the SDD is shown in Figure 5.3(a).



(a) Stationary dynamic deflectometer (SDD)



(b) Expanded view of the SDD loading system and layout of sensors

Figure 5.3: General SDD testing arrangement

The hydraulic system of the SDD can apply both a static hold-down force and a dynamic force to the test slab. The repeated dynamic force is applied to the slab using a loading frame with three circular steel loading pads as illustrated in Figure 5.2. The three-pad loading system

avoids instability problems. An expanded view of the SDD loading platform and the locations of the load cell, accelerometers, and LVDTs is shown in Figure 5.3(b).

5.4.2 Foundation Properties

A typical three-layer rigid pavement system, which consisted of natural subgrade, asphalt stabilized base and concrete slab, was examined in this study. The performed tests for foundation properties are illustrated in Figure 5.4.

Subgrade

The accelerated full-scale tests were performed at a site at the University of Texas at Austin Pickle Research Campus. A natural subgrade site of 60 ft by 120 ft was scraped, leveled and roller compacted. The natural subgrade soil is a clayey-sand that can be classified as AASHTO Class A-2-6 based on sieve analysis and plastic characteristics. The average liquid limit is 37%, and the average plastic limit is 19%. To investigate the material properties of the subgrade, three in-situ subgrade tests were performed using TxDOT equipment: 1) the dynamic cone penetration (DCP), 2) the portable falling weight deflectometer (PFWD), and 3) the nuclear density. DCP tests for 36 points were performed, and an average California bearing ratio (CBR) value of 16.7 and a correlated elastic modulus of approximately 15,400 psi were obtained. The PFWD test data were used for checking uniformity for the site, and the PFWD data were compared to DCP results. Compared to the DCP results, the PFWD data showed an identical tendency for a given location but the elastic modulus was about 65% of DCP average value. The data from the DCP tests were used in this study. Density and water contents of the subgrade were measured using the nuclear density test at the same 36 test locations. The average dry density of the subgrade soil was 95 lb/ft³, and the average water content was 18%. All subgrade testing was performed one to two days before the asphalt base placement to reduce the possibility of material changes due to environmental conditions.

Asphalt Stabilized Base

The 4-in-thick asphalt stabilized base was constructed on the compacted subgrade in accordance with TxDOT specification item 345. The maximum aggregate size was 1 in., and the asphalt content was 4.6%. To obtain the elastic modulus of the asphalt-stabilized base, the falling weight deflection (FWD) test was performed at the same 36 locations used for subgrade testing. The back-calculated average elastic modulus of asphalt-stabilized base was 270 ksi with a coefficient of variance of 0.13. The average density of the asphalt-stabilized base from core samples was 94 lb/ft³ with a coefficient of variance of 0.042.

5.4.3 Full-Scale Concrete Slab Properties

The same concrete mixtures used in the laboratory beam fatigue testing were used for the field slabs. Six full-scale concrete slabs were tested with different age conditions: four SRG slabs and two LS slabs. The dimensions of the full-scale concrete slabs were 12 ft by 12 ft by 6 in.. All slabs were cast and tested at the Pickle Research Campus, The University of Texas at Austin, during the summer of 2003. Two slabs were cast from the same load, and the curing compound was applied on the top surfaces in accordance with TxDOT specifications.



(a) Dynamic cone penetration (DCP) testing on subgrade



(b) Nuclear density testing on subgrade



(c) Falling weight deflection (FWD) testing on asphalt stabilized base

Figure 5.4: Photographs of foundation testing at the full-scale slab testing

Field-Cured Specimens Static Tests

To determine the mechanical properties of the concrete mixture used in the field slabs, 4-in. by 8-in. cylinders and 6-in. by 6-in. by 20-in. beams were cast at the time of slab casting. All cylinders and beams were cured in a wet sand bed adjacent to the slab testing site, and the temperature histories were monitored to compare the maturity values with field slabs. The recorded temperature differences between the temperature at the middle of the slab and the temperature of the specimen were negligible (less than $\pm 3^{\circ}\text{F}$) for all test slabs.

Core Splitting Tensile Test

Cores were taken and tested in splitting tension to compare the slab strength to the sand-cured strength. The 4 in. by in. cores were taken and tested in splitting tension at 2, 7, and 28 days. Conservatively, it was assumed that the strengths from sand-cured specimens were the strengths corresponding to the full-scale slabs.

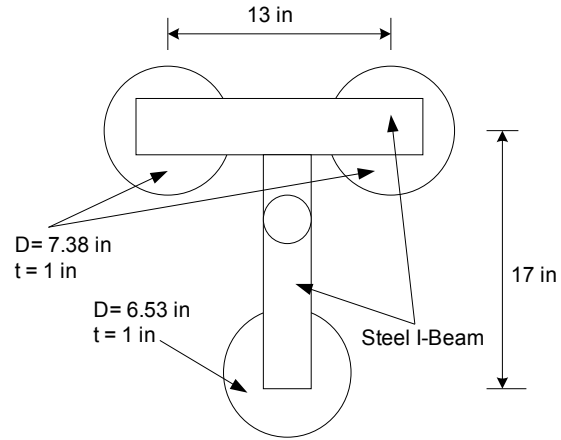
Static Partial Loading Tests on Concrete Slab

Before the application of cyclic loading, each slab was loaded statically using the same load arrangement until a static hold-down force (9-kips) was reached to obtain a static load-displacement curve to back calculate the subgrade reaction modulus (k -value). Based on the measured static load-displacement relationships, the subgrade reaction modulus (k -value) for each slab was back-calculated using the EverFE program (1998).

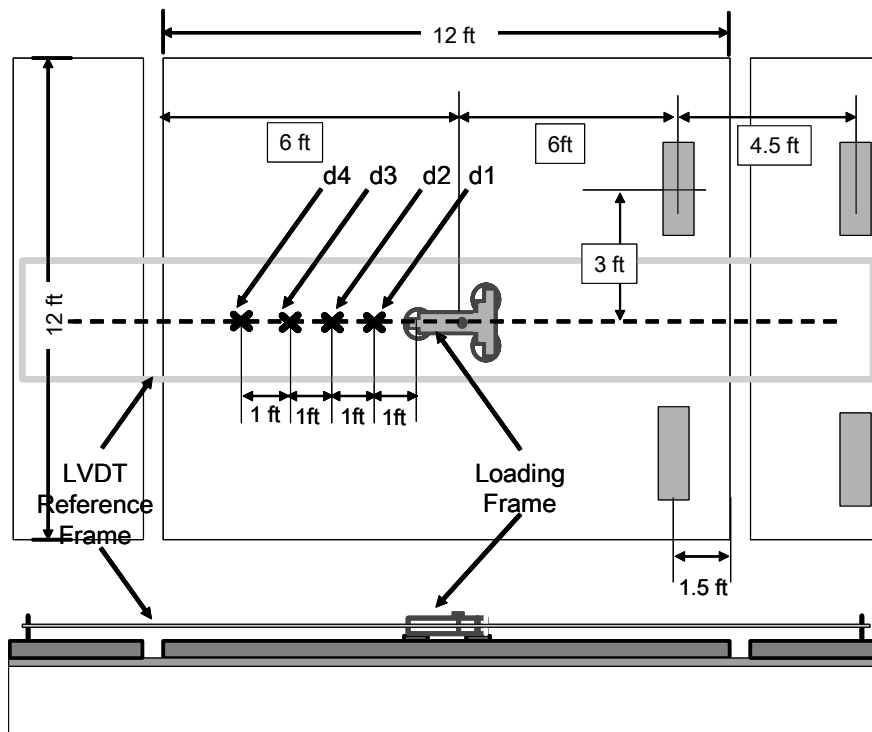
5.4.4 Super-Accelerated SDD Slab Testing Procedure

The static and dynamic loads from the SDD were applied at the center of the concrete pavement through a loading frame to reduce the edge loading effect. The field arrangement of super-accelerated testing is illustrated in Figures 5.5 through 5.7. To avoid the instability of the SDD system, a minimum hold-down force of about 30% of the maximum dynamic load was required. An initial 9-kip static hold-down force was applied, and then the continuous dynamic force was applied at a rate of 1200 cycles per minute (20 Hz). A load cell was connected the SDD to the loading frame, and it was used to measure both the applied static and dynamic forces. The surface displacement profile along the centerline was captured during the entire test period using two types of sensors. First, three accelerometers were used to measure the dynamic motion of the pavement. Second, three other LVDTs were also used for the measurement of the permanent deformation of the pavement. In order to make accurate displacement readings, the LVDTs must be mounted on a reference frame. The reference frame was 3 ft by 18 ft and was supported by bolts as shown in Figure 5.5(b).

The number of cycles to the appearance of the first visible crack was used for the definition of the number of load repetition to failure (N). Even after the occurrence of a visible crack, each test slab was loaded continuously until the visible crack propagated to the surface of the edge of the concrete slab, full-depth. If a full-depth edge crack could not be observed after a reasonable number of loading cycles was applied, the testing was terminated. After testing each slab, the dynamic displacement data from the accelerometers were plotted against the number of applied load repetitions. In general, the dynamic displacement increased rapidly as the concrete slab approached failure.

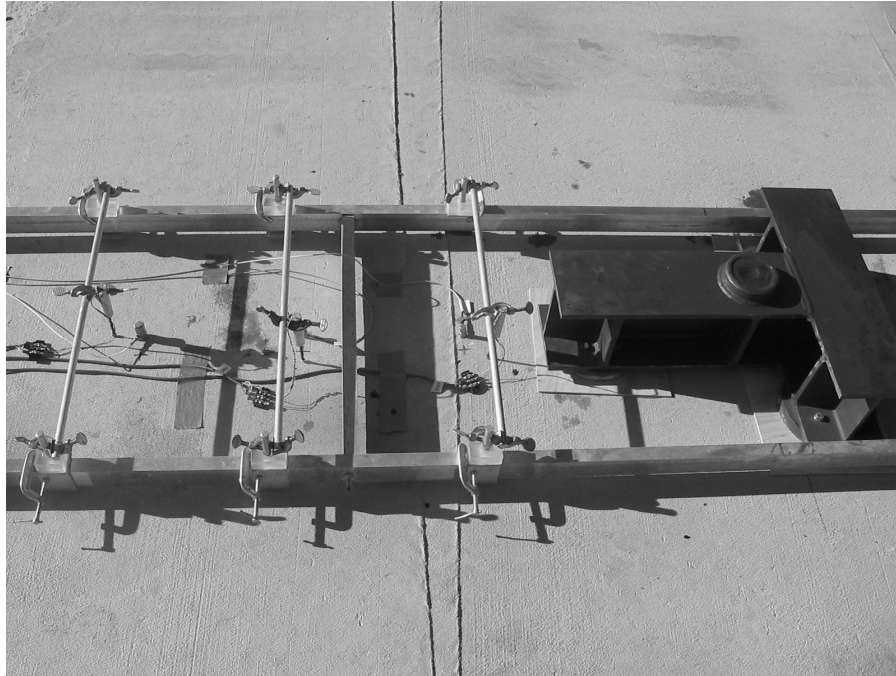


(a) Configuration of loading pads



(b) Plan view of instrumentation

Figure 5.5: Static and dynamic instrumentation



(a) Arrangement of loading frame and instrumentation prior to the testing



(b) Loading mechanism in position over loading frame

Figure 5.6: Photograph of field arrangement of SDD super-accelerated testing



(a) SDD positioned over testing slab



(b) Super-accelerated fatigue testing system using SDD

Figure 5.7: Photograph of full-scale slab fatigue testing in progress

5.4.5 Super-Accelerated Full-Scale Concrete Slab Testing Results

All full-scale slabs failed under the SDD super-accelerated testing. The test results are summarized in Table 5.2. The maximum and minimum stresses at the bottom of the slabs were calculated using EverFE software based on static properties of the slabs.

Table 5.2: Super-accelerated full-scale slab fatigue testing results

Slab Number	Agg. Type	Age of Test (Days)	Avg. Beam Modulus of Rupture (psi)	Max. Applied Cyclic Load (kips)	Min. Applied Cyclic Load (kips)	Calculated Maximum Stress (psi)	Calculate d Minimum Stress (psi)
1	SRG	2	537	27.0	9.0	466	202
2	SRG	28	682	30.0	9.0	542	216
3	SRG	8	609	30.0	9.0	528	209
4	SRG	29	711	30.0	9.0	598	244
5	LS	7	566	30.0	9.0	503	215
6	LS	28	682	30.0	9.0	560	229
Slab Number	Max. Stress Level	Min/Max Stress Ratio	Number of Cycles to First Visible Crack, <i>N</i>	Equivalent No. of Cycles to Failure, <i>EN</i>	No. of Cycles to End of Testing	Edge Crack Depth at the End of Testing	
1	0.88	0.43	100,700	711	180,200	Whole	
2	0.81	0.40	140,300	1,225	223,000	Whole	
3	0.86	0.39	335,900	2,350	600,000	Partial	
4	0.84	0.41	360,500	1,899	600,000	Partial	
5	0.89	0.43	78,800	618	92,000	Whole	
6	0.82	0.41	463,300	2,202	600,000	Partial	

Failure Mode

For all slabs, the first visible crack was observed at the top surface near the loading point, and the main failure crack pattern coincided with the maximum stress path as shown in Figure 5.8(a). After a substantial number of cycles, the edge cracks could usually be visually observed at the bottom of the slabs and then they propagated to the top surface. Three slabs showed more than one fully propagated full-depth edge crack at the end of testing, while the other three slabs only had partial-depth cracks at the edge, and therefore tests were terminated at 600,000 cycles.

The observed full- and partial-depth edge cracks at the end of the testing are presented in Figure 5.8(b) and 5.8(c), respectively. It is noted that the slabs tested under higher stress level (Slabs No. 1 and No. 5) had full-depth cracks at the edges, which propagated from interior of the slabs.

Displacement Measurement

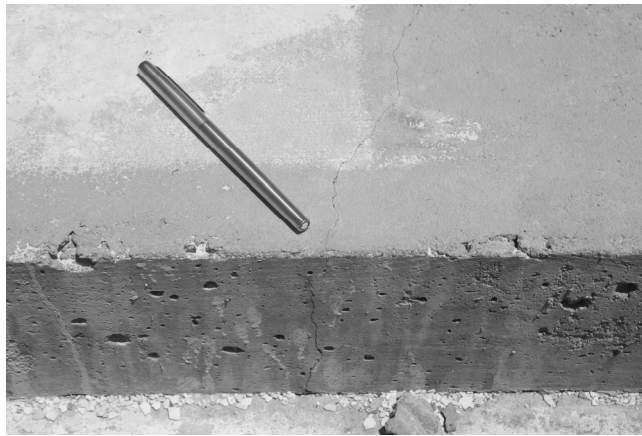
The dynamic displacement variations for test slabs are illustrated in Figure 5.9. The measured dynamic displacement data were normalized with respect to the initial dynamic displacement for comparison. For all test slabs, the dynamic displacements increased over the entire fatigue life. In general, the dynamic displacement after the first visible crack increased at a higher rate before cracking. In the case of Slabs No. 1 and 5, the occurrence of the first visible crack occurred simultaneously with the abrupt change of displacement rate. The increase in dynamic displacement before the first crack was due to the sum of the plastic deformation of concrete slabs and permanent deformation of foundation. It is noted that Slab No. 1, which had the strongest subgrade, showed basically no change in dynamic deflection before the first visible crack. The stress redistribution phenomenon was also observed. In spite of the stiffness reduction of slabs after the cracking, the full-scale rigid pavement system was still able to deliver stresses to the foundation (asphalt base and subgrade).

Comparison of Field Slab and Laboratory Beam S-N Curve

A comparison of the super-accelerated full-scale slab fatigue testing and laboratory beam fatigue testing is provided in Figure 2.16. Fatigue life based on the first crack criteria for the full-scale slabs was found to be approximately 50% higher in log scale than the fatigue life of laboratory beams. However, the SDD testing used a significantly higher minimum-to-maximum stress ratio ($R=0.40$) than laboratory beam testing ($R=0.10$). Therefore, the correction of the S-N curves between those two data sets is inevitably required. Applying the concept of equivalent fatigue life (EN) as described previously, the corrected slab data points were essentially on the beam S-N curves. In other words, the laboratory beams and full-scale field slabs have an identical S-N relationship after the correction for the variance of stress ratio. This is a very important finding.



(a) Plan view of the failed slabs

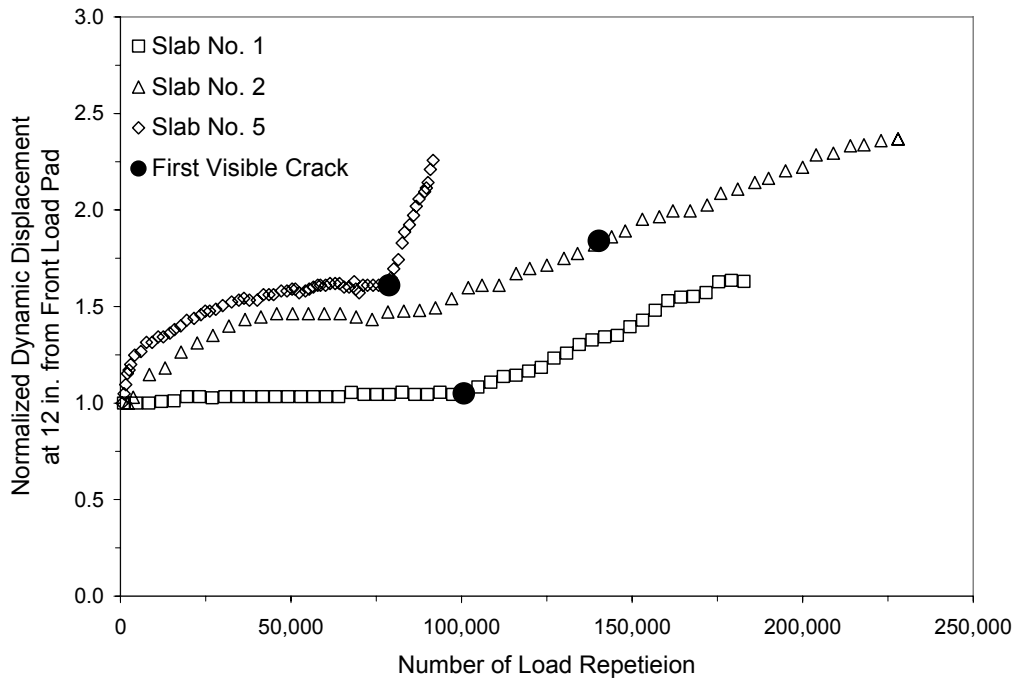


(b) Full-depth edge crack after fatigue failure

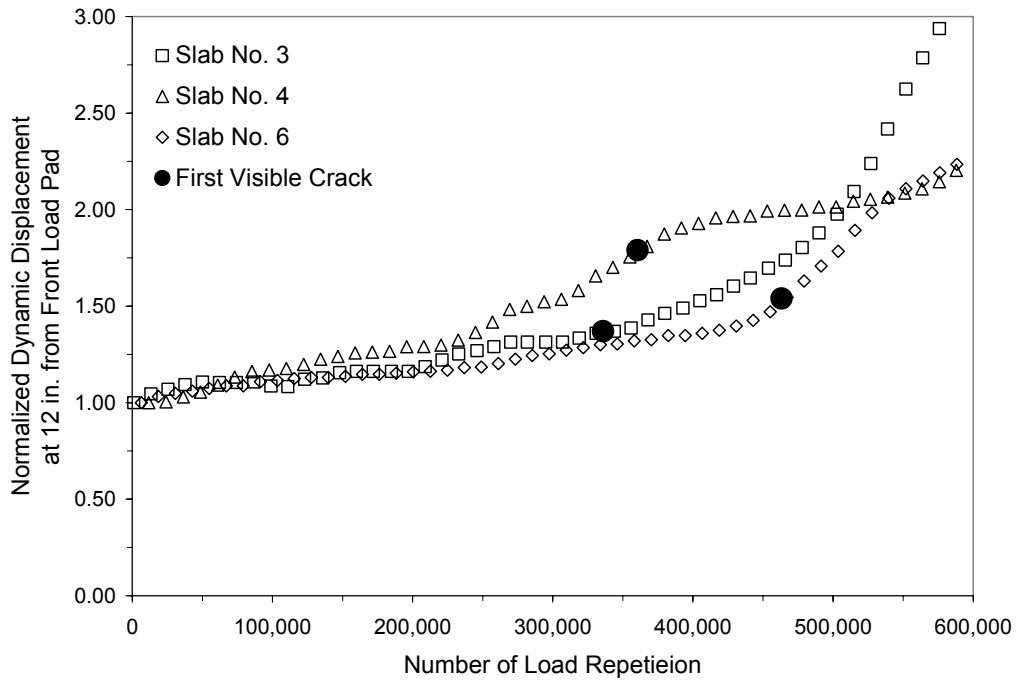


(c) Partial-depth edge crack after fatigue failure

Figure 5.8: Photographs of failed slabs after fatigue testing



(a) Slabs with partial-depth edge cracks



(b) Slabs with full-depth edge cracks

Figure 5.9: Variation of normalized dynamic displacement for full-scale slabs

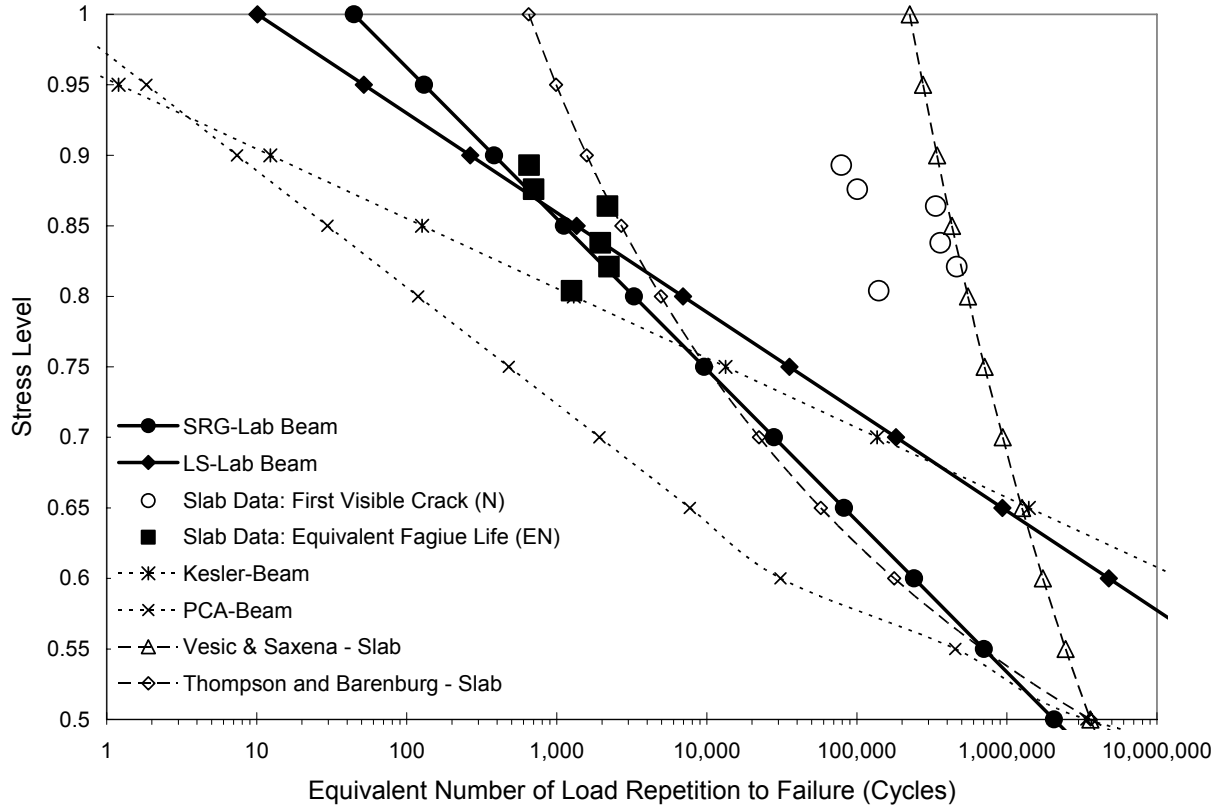


Figure 5.10: Comparison of laboratory beam and full-scale slab fatigue curves

5.5 Opening-to-Traffic Flexural Strength Criteria

This section presents the development of a conceptual model for evaluating the effect of early opening to traffic on the life of a PCCP. Using the proposed mathematical model, a series of numerical simulations were performed and the results were analyzed.

5.5.1 Mathematical Model

In PCCP design, the most commonly used fatigue-cracking criterion is based on Miner's linear damage theory. The consumed life of PCCP is normally expressed on the assumption of Miner's linear damage theory (Miner, 1945) as shown in Equation 5.6. The fatigue failure may occur when the sum of damage for all stress levels reaches a certain critical value, namely 1 in the case of Miner's theory. If Miner's law controls the life of a PCCP, the total damage of a PCCP can be defined as Eq. (5.6).

$$D = \sum_{i=1}^m \frac{n_i}{N_i} \leq 1 \quad (5.6)$$

where

D = total damage,

m = number of different stress levels,

n_i = number of cycles at stress level i , and
 N_i = the total number of stress cycles to failure at stress level i .

For the design process, the various wheel (axle) loads present in mixed traffic is transformed into equivalent load applications based on a standard axle of 18-kips. Thus, Equation 5.6 can be simplified to one stress level load on the 18-kips ESAL as follows:

$$D = \sum_{i=1}^m \frac{W_{18-i}}{W_{18-d}} \leq 1 \quad (5.7)$$

where,

D = total damage,
 d = age for achieving design strength ,
 i = time interval,
 W_{18-i} = actual number of ESAL's experienced during a time i ,
and
 W_{18-d} = design ESAL for a set of conditions defining a performance limit, i.e., minimum serviceability.

For developing the early opening criteria, the use of Equation 5.6 was varied slightly because the conventional application has different stress levels resulting from mixed traffic. These applications occur after the concrete has acquired its desired strength, i.e., strength invariant. Because early opening occurs when the strength and modulus of elasticity are changing rapidly, each day must be viewed as a separate period. Thus, Equation 5.7, which was simplified by a using single load based on the ESALs, is transformed to referent the different time periods as shown in Equation 5.8.

$$D = \sum_{i=a}^m \frac{n_i}{N_i} \quad (5.8)$$

where

D = total damage,
 a = age of concrete at opening,
 m = age of rigid pavement,
 n_i = number of load repetition during i^{th} -day, and
 N_i = number of load repetition to failure based on i^{th} -day strength.

Using Equation 5.8 and the fatigue characteristics of a PCCP, the life of PCCPs that have the different first age of loading conditions can be calculated. Combining with Miner's law and the fatigue relationship of a PCCP, the loss of life due to early opening to traffic due to loading prior to achieving design strength can be derived as Equation 5.9.

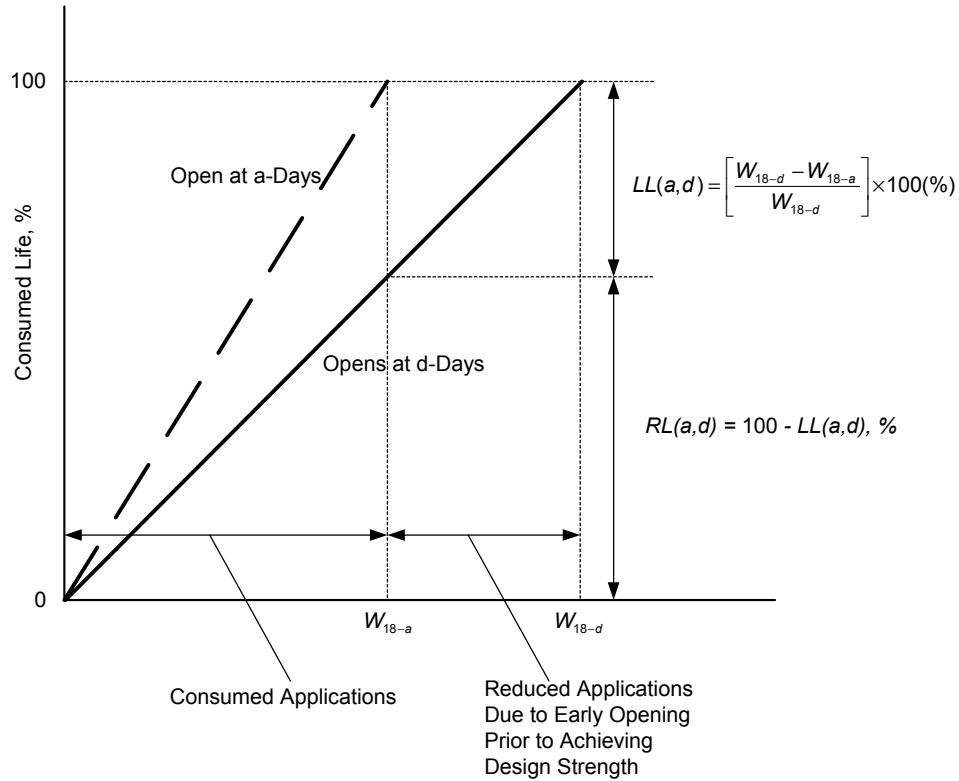
$$LL(a,d) = \left[\frac{W_{18-d} - W_{18-a}}{W_{18-d}} \right] \times 100(\%) \quad (5.9)$$

where

a = opening age of PCCP (days),
 d = age achieving design strength = 28-days,
 W_{18-a} = number of load repetition to failure when a PCCP opens at a -day, and

W_{18-d} = number of load repetition to failure when a PCCP opens at d -day.

Figure 5.11 shows the conceptual diagram for the loss of life of a PCCP due to early opening prior to achieving the design; the horizontal axis represents the number of load application while the vertical axis represents the consumed life in terms of percentile value with respect to the total life of a PCCP.



where, LL = Loss of life
 RL = Remaining life
 a = Opening age of PCCP, days
 d = Age achieving design strength, days
 W_{18-d} = Number of load repetition to failure when a PCCP opens at a -days
 W_{18-a} = Number of load repetition to failure when a PCCP opens at d -days based on design strength

Figure 5.11: Conceptual diagram of the loss of life

5.5.2 Regression Analysis

The regression analyses for the results set considering possible input variables were performed to predict the value of loss of life in general.

Assumptions for Mathematical Model

Various conditions for simulations were assumed to quantify the loss of life (*LL*) due to early opening prior to achieving design strength in this study. Major assumptions for the mathematical model are as follows:

- Miner's linear damage theory is valid.
- The age increment is one day.
- Concrete material is homogeneous and isotropic.
- The strength of concrete remains constant for one day. Static strength results from laboratory testing are valid.
- The flexural strength and elastic modulus of the concrete changes daily between the age at opening (*a*) and the age design strength is met (*d*).
- The fatigue relationships developed from laboratory testing are valid. The developed S-N curves for each aggregate are valid for all ages.
- Load applications after an age of 28 days have the same damage as values at 28 days, i.e., no strength gain after 28 days.
- The Westergaard equations are valid for stress calculation. Circular loading condition is applicable for edge condition.
- 18,000 lbs of equivalent single-axle load (ESAL) is valid for stress calculations. The radius of loading is 6 in.
- Uniform traffic occurs in terms of number of load repetitions per day.

Input Variables

Extensive sensitivity analyses were performed for a variety of conditions using the analysis procedures described in previous section. The combination of all variables resulted in 7,776 data points. The values of each variable selected in this study are summarized in Table 5.3.

Table 5.3: Summary of used input variables

Variable	Selected Input Levels
Coarse aggregate type	SRG and LS
Fatigue equation	Equation (5.4) and (5.5)
Static strength parameters	Modulus of Rupture and Elastic Modulus
Curing temperature (°F)	50, 75, 100
Thickness of PCCP (in.)	6, 8, 10, 12
Subgrade modulus, <i>k</i> (psi/in.)	100, 300, 500
Edge loading ratio, (%)	0, 20, 40
Number of load repetition (per day)	2500, 5000, 7500, 10000
Opening age (days)	1, 2, 3, 4, 5, 6, 7, 14, 28
Total number of simulation	7,776 data points

Regression Analysis Results

The developed mechanistic calculation model generated a large number of data sets based on variable selections. To establish a statistically meaningful regression equation, a partial log expression was used for data analyses as shown in Equation 5.10.

$$\log(LL) = A + B\log(k) + C\log(h) + D\log(ESAL) + E\log(MR) + F(Edge) \quad (5.10)$$

where

A, B, C, D, E, F = regression coefficient,

LL = predicted loss of life due to early opening (%),

k = subgrade reaction modulus (pci),

h = pavement thickness (in.),

$ESAL$ = number of 18-kips ESAL per day,

MR = modulus of rupture at opening of pavement (psi), and

$Edge$ = ratio of edge loading (%)

= number of circular edge loading / total number of loading

= 0 for interior loading.

The least squares linear regression analysis was used to determine the best fit for the coefficients in Equation 5.10. The adjusted R^2 values are in an acceptable range (0.84 to 0.91). In order to find the value of the required minimum flexural strength at opening, Equation 5.10 is transposed into Equation 5.11.

$$\log(MR) = A' + B'\log(k) + C'\log(h) + D'\log(ESAL) + E'\log(LL) + F'(Edge) \quad (5.11)$$

where

A', B', C', D', E', F' = regression coefficients,

MR = minimum required modulus of rupture at opening of pavement (psi), and

LL = allowable loss of life due to early opening (%)

The calculated data using developed model can be approximated with the following generalized English unit equations:

$$\log(MR) = 4.56 - 0.18\log(k) - 2.57\log(h) + 0.11\log(ESAL) - 0.13\log(LL) + 0.008(Edge) \quad (5.12)$$

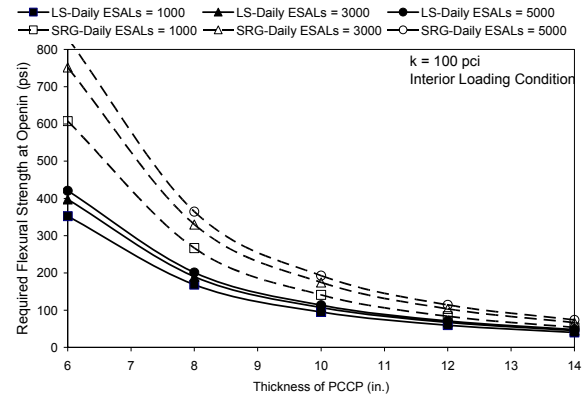
for LS

$$\log(MR) = 4.81 - 0.19\log(k) - 2.86\log(h) + 0.19\log(ESAL) - 0.26\log(LL) + 0.009(Edge) \quad (5.13)$$

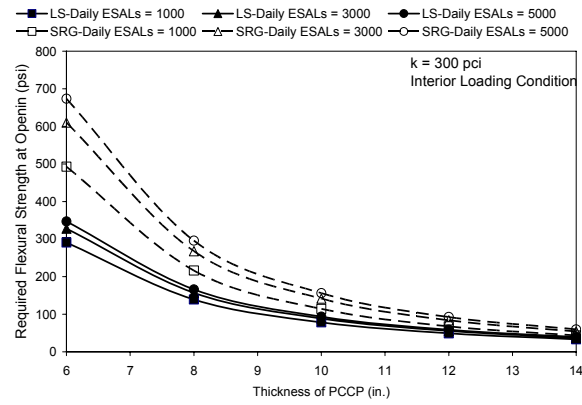
for SRG

By entering $LL=1\%$ (the allowable fatigue damage of 1% at early age) into Equation 5.12 and 5.13, the minimum required flexural strength at the time of opening could be calculated.

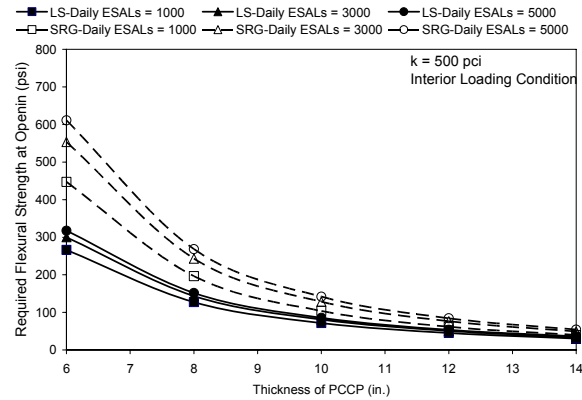
Because of reduced static and fatigue performance of SRG coarse aggregate mixture, all SRG mixtures require higher opening flexural strength than that of LS mixtures as expected. While the calculated required flexural strength value for opening is dependent on various variables, the current opening criterion for normal paving mixture in TxDOT specifications (450-psi flexural strength) is satisfactory for most interior loading conditions.



(a) $k = 100$ pci, interior loading condition

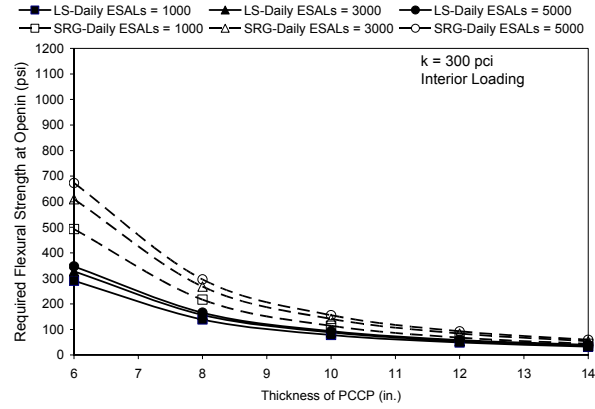


(b) $k = 300$ pci, interior loading condition

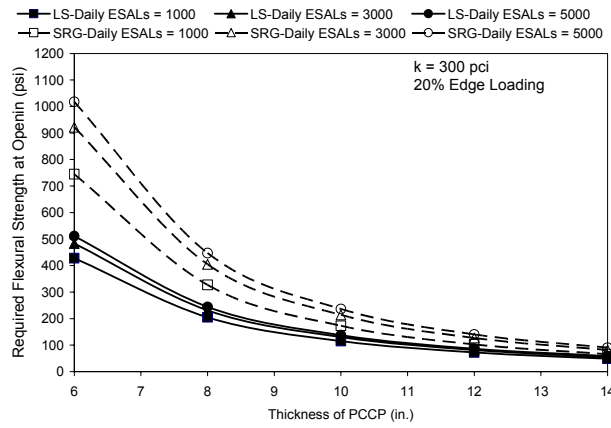


(c) $k = 500$ pci, interior loading condition

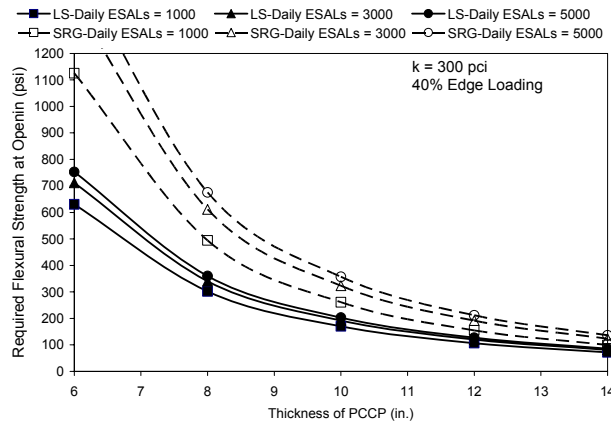
Figure 5.12: Sensitivity analysis of required flexural strength for opening with various subgrade reaction modulus (interior loading condition)



(a) Interior loading condition, $k = 300$ pci



(b) 20% edge loading condition, $k = 300$ pci



(c) 40% edge loading condition, $k = 300$ pci

Figure 5.13: Sensitivity analysis of required flexural strength for opening with various edge loading ratio ($k = 300$ pci)

The presence of edge loading requires a significant increase in minimum flexural strength value for opening. The required flexural strength at opening rapidly increases with an increase in the edge loading ratio. SRG mixtures are more sensitive for the change in edge loading ratio than that of LS mixtures. Forcing traffic toward the edge will result in greater early fatigue damage. Considerations on the edge loading condition should be made. Reducing critical edge stresses is the key factor in the prevention of fatigue damage at early ages; for example, reinforcing dowels between outer lane and shoulder should be considered. In spite of this edge loading effect, the current 450-psi opening criteria is still reasonable except for very thin SRG pavements.

A factor of safety is incorporated into the flexural strength criteria by not accounting for the strength gain during each 24-hour age increment, which is significant at very early ages. The continuous strength increase will be achieved during the application of loading in a day. Another factor of safety is using a laboratory fatigue curves. Comparing with the field *S-N* curves based on serviceability failure criterion, the developed fatigue curves in this study are very conservative, although their failure definition is different.

5.6 Summary

Concrete pavements are subjected to many traffic-load repetitions prior to achievement of their full design strength. The effect of early opening to traffic on the life of portland cement concrete pavement systems was evaluated using experiments and mathematical model.

To quantify the loss of life due to early opening of a rigid pavement system, an appropriate fatigue equation is fundamentally required. A series of laboratory fatigue tests was performed on simply supported beams to develop appropriate fatigue relationships for typical, normal strength Texas paving concrete mixture designs. After completion of the laboratory testing, accelerated fatigue tests on full-scale concrete slabs were performed under constant cyclic loading.

The concept of equivalent fatigue life was applied to correct the effect of the different stress ratios between field and laboratory testing. The laboratory beams and full-scale field slabs showed an almost identical fatigue relationship after the correction for the variance of stress ratio.

On the basis of Miner's hypothesis of linear accumulated damage, an analytical model for the numerical simulation for the prediction of the loss of life of a portland cement concrete pavement due to early opening was developed. The numerical simulations were performed for the various assumptions and considerations for field conditions. The current opening criteria used by the Texas Department of Transportation appear to be reasonable based on the sensitivity analysis results.

Chapter 6. Conclusions

This chapter provides a summary of the work undertaken over the course of this study. The following conclusions are made on the basis of the results of this study.

6.1 Temperature Control

The study developed mitigation techniques to control the in place temperature development of early-age concrete. Longer lasting PCC pavements will be produced if the assumptions made during pavement design development are achieved in the field. This study proposes a method to integrate the design assumptions to the construction process by means of an end-result temperature control specifications.

A general hydration model for cementitious materials and a model to predict the temperature gain in hardening concrete is developed and calibrated. The temperature prediction model was calibrated for field conditions with data collected from seven concrete paving projects. The model accounts for different pavement thicknesses, mixture proportions, cement chemical compositions, cement fineness, amount of cement, mineral admixtures, material types, climatic conditions, and different construction scenarios. The temperature prediction model will enable the development of performance based specifications to guard against premature concrete failures. This model will further provide the designer, contractor, and specification developer with the means to evaluate and quantify the effect of most of the various complex interactions that affect the concrete temperature development during early-ages.

A model to predict initial and final setting of hardening concrete is presented, and calibrated, with data collected under laboratory and field conditions. The effects of concrete temperature, different cements, and mineral admixtures on the initial and final setting times are characterized.

6.2 Moisture Effects

Mathematical models were developed for the calculation of moisture and temperature profiles to help investigate the effect of different combinations of climate, construction, and materials on the development of the moisture and temperature profiles and their subsequent effects on early-aged cracking. The calculated moisture and temperature profiles using the moisture diffusivity and thermal conductivity models corresponded to the measured data.

Spalling distress is strongly correlated to pre-existing horizontal delaminations that occur within 1 in. of the pavement surface. The cause of the shallow, horizontal delaminations that occur within the top 1 in. of the pavement surface is primarily from early-age nonlinear shrinkage strains in addition to temperature variations through slab depth. Thus, the factors of the most importance are those related to the effectiveness of the curing medium in minimizing moisture loss during the hydration of the concrete and the bond strength between the aggregate and the paste. By increasing the effectiveness of the curing system, moisture gradients near the surface are substantially reduced and delamination stresses minimized.

6.3 Sensitivity Analysis of CRCP Computer Program

The sensitivity of the design variables to the behavior of continuously reinforced concrete pavement (CRCP) has been investigated using mechanistic models of CRCP. The practical

ranges of the design variables have been selected and the typical values of the variables have been determined.

In the sensitivity analysis, one variable is selected and varied within the practical range while the other variables remain at their typical values, and the analysis results such as mean crack spacing, crack width, and steel stress at crack are obtained. From this study, the relationships between the design variables and the CRCP behavior have been obtained.

It has been found that the zero-stress temperature and the coefficient of thermal expansion of concrete are the most sensitive design or materials variables, and the steel bar diameter and the stiffness of underlying layers are the least sensitive variables. The other variables can be defined as moderately sensitive variables. Because engineers have only limited resources and time to use in estimating a large number of design variables, the findings described in this report can be applied to aid in solving real problems more efficiently.

6.4 Early Opening Criteria

The effect of early opening to traffic on the life of portland cement concrete pavement systems was evaluated using experiments and mathematical model. To quantify the loss of life due to early opening of a rigid pavement system, an appropriate fatigue equation is fundamentally required. A series of laboratory fatigue tests was performed on simply supported beams to develop appropriate fatigue relationships for TxDOT's Class P concrete. After completion of the laboratory testing, accelerated fatigue tests on full-scale concrete slabs were performed under constant cyclic loading.

The concept of equivalent fatigue life was applied to correct the effect of the different stress ratios between field and laboratory testing. The laboratory beams and full-scale field slabs showed an almost identical fatigue relationship after the correction for the variance of stress ratio.

On the basis of Miner's hypothesis of linear accumulated damage, an analytical model for the prediction of the loss of life of a portland cement concrete pavement due to early opening was developed. The numerical simulations were performed for the various assumptions and considerations for field conditions. The current opening criteria used by the Texas Department of Transportation appear to be reasonable based on the sensitivity analysis results.

Appendix: Guidelines for Acceptance and Opening to Traffic Criteria for New PCC Pavements.

Over the years, the Center for Transportation Research at The University of Texas at Austin, under the support of the Texas Department of Transportation (TxDOT), has conducted various research projects on materials, design, construction and analysis of portland cement concrete (PCC) pavement, more specifically continuously reinforced concrete pavement (CRCP), to improve its performance. Based on the results from 0-1700 project as well as a review of the literature, recommendations can be divided into two categories: acceptance criteria for temperature and opening to traffic criteria for new PCC pavements.

Concrete Temperature Restriction

The concrete temperature at early ages has a significant effect on long-term performance of PCC pavement. Under research project 0-1700, a concrete temperature model to predict initial and final setting of hardening concrete was developed and calibrated based on field data collected from seven CRC construction sites visited during this study. Concrete temperatures measured in the field were compared to the temperatures predicted with the temperature model. Based on the average r^2 values, 78% of the measured in-place concrete temperatures can be explainable by the temperature prediction model. The error obtained between the measured and predicted maximum in-place concrete temperature ranged between -4.6% and 3.4%.

However, the predicted concrete placement times and elapsed times before maximum concrete temperatures and differentials take place, and the depths of maximum temperature are quite different from those observed in the actual pavement.

It is recommended that further efforts be made to improve the accuracy of the temperature prediction models. Even though the effect of concrete placement temperature on long-term CRCP performance has been known and documented, it hasn't been accurately quantified. Until accurate, quantifiable information becomes available, it is recommended that no modifications be made to the current specifications on concrete temperature restrictions.

Opening to Traffic Criteria

The current Texas Department of Transportation (TxDOT) concrete pavement thickness design is based on a 28-day third-point loading flexural strength of 680 psi. However, the Item 360.4.K of the TxDOT specification requires the minimum opening flexural strength of 450 psi or a compressive strength of 2,800 psi. Therefore, when a PCC pavement is opened to traffic before 28-days, the question arises how much damage is done to pavement, or even how much potential life is lost by early opening to traffic.

Under the 0-1700 research project, the effect of early opening to traffic on the life of portland cement concrete pavement systems was evaluated using experiments and mathematical model. A series of laboratory fatigue tests was performed to develop appropriate fatigue relationships for typical, normal strength Texas paving concrete mixture designs. After completion of the laboratory testing, accelerated fatigue tests on full-scale concrete slabs were performed under constant cyclic loading.

The concept of equivalent fatigue life was applied to correct the effect of the different stress ratios between field and laboratory testing. The laboratory beams and full-scale field slabs showed an almost identical fatigue relationship after the correction for the variance of stress ratio.

On the basis of Miner's hypothesis of linear accumulated damage, an analytical model for the numerical simulation for the prediction of the loss of life of a portland cement concrete pavement due to early opening was developed. The numerical simulations were performed for the various assumptions and considerations for field conditions. The current opening criteria used by the Texas Department of Transportation appear to be reasonable based on the sensitivity analysis results. Therefore, it is also recommended that no modifications be made to the current specifications on early opening to traffic.

References

- ASTM C 1074, “Standard practice for estimating concrete strength by the maturity method,” American Society for Testing and Materials, Pennsylvania, 1998.
- ASTM C 403, “Standard Test Method for Time of Setting of Concrete Mixtures by Penetration Resistance,” ASTM C 403-95, Annual Book of ASTM Standards, American Society for Testing and Materials, Pennsylvania, 1998.
- Bay, J. A., K. H. Stokoe, II., and J. D. Jackson. Development and Preliminary Investigation of a Rolling Dynamic Deflectometer. In Transportation Research Record 1473, TRB, National Research Council, Washington, D.C., 1995, pp. 43–54.
- Bay, J. A., K. H. Stokoe, II., B. F. McCullough, and D. R. Alexander. Profiling Flexible Highway Pavement Continuously with Rolling Dynamic Deflectometer and at Discrete Points with Falling Weight Deflectometer. In Transportation Research Record 1655, TRB, National Research Council, Washington, D.C., 1999, pp. 74–85.
- Bazant, Z.P., “Thermodynamic Theory of Deformations of Concrete with Explanation of Drying Creep.” American Concrete Institute Symposium on Designing for Effects of Creep, Shrinkage and Temperature, SP 27, 1969.
- Branco, F.A., R.A. Mendes, and E. Mirabell. Heat of Hydration Effects in Concrete Structures. ACI Materials Journal, Vol. 89, No. 2, pp. 139-145, 1992.
- Byfors, J. “Plain Concrete at Early Ages,” Research 3:80, Swedish Cement and Concrete Research Institute, Stockholm, Sweden, 1980.
- Chiang, Chypin, B. F. McCullough, and W. Ronald Hudson. (1975). A sensitivity Analysis of Continuously Reinforced Concrete Pavement Model CRCP-1 for Highways. Research Report 177-2, Center for Transportation Research, The University of Texas at Austin.
- Chapman, A.J., Fundamentals of Heat Transfer. Macmillan Inc., New York, New York, 1982.
- Chen, Y., and Odler, I., “On the Origin of Portland Cement Setting,” Cement and Concrete Research, Vol. 22, No. 6, pp. 1130-1140, 1992.
- Davis, W. G., G. M. Turkiyyah, and J. P. Mahoney. EverFE-Rigid Pavement Three-Dimensional Finite Element Analysis Tool. In Transportation Research Record 1629, TRB, National Research Council, Washington, D.C., 1998, pp. 41–49.
- Dossey, T., and B. F. McCullough. (1991). Characterization of Concrete Properties with Age. Report 1244-2, Center for Transportation Research, The University of Texas at Austin.

- Dossey, T., McCullough, B.F. and Dumas, A., "Effects of Aggregate Blends on the Properties of Portland Cement Concrete Pavements," Research Report 1224-8, Center for Transportation Research, The University of Texas at Austin, August 1994.
- Hankins, K., Suh, Y.C., and McCullough, B.F., "Field Evaluation of Coarse Aggregate Types: Criteria for Test Sections," Research Report 422/1244-1, Center for Transportation Research, The University of Texas at Austin, January 1991.
- Kesler, C. E. Effect of Speed of Testing on Flexural Fatigue Strength of Plain Concrete. Proceedings, Thirty-Second Annual Meeting, Highway Research Board, Washington, D.C., V. 32, 1953, pp. 251-258.
- Kim, S. M., M. C. Won, and B. F. McCullough. (1997). Development of a Finite Element Program for Continuously Reinforced Concrete Pavements. Report 1758-S, Center for Transportation Research, The University of Texas at Austin.
- Kim, S. M., M. C. Won, and B. F. McCullough. (1998). "Numerical Modeling of Continuously Reinforced Concrete Pavement Subjected to Environmental Loads." In Transportation Research Record 1629, TRB, National Research Council, Washington, D.C., pp. 76~89.
- Kim, S. M., M. C. Won, and B. F. McCullough. (2000). "Three-Dimensional Analysis of Continuously Reinforced Concrete Pavements." In Transportation Research Record 1730, TRB, National Research Council, Washington, D.C., pp. 43~52.
- Kim, S. M., M. C. Won, and B. F. McCullough. (2001). CRCP-9: Improved Computer Program for Mechanistic Analysis of Continuously Reinforced Concrete Pavements. Report 1831-2, Center for Transportation Research, The University of Texas at Austin.
- Ma, James, and B. F. McCullough. (1977). CRCP-2, An Improved Computer Program for the Analysis of Continuously Reinforced Concrete Pavements. Report 177-9, Center for Transportation Research, The University of Texas at Austin.
- McCullough, B. F., A. A. Ayyash, W. R. Hudson, and J. P. Randall. (1975). Design of Continuously Reinforced Concrete Pavements for Highways. Report NCHRP 1-15, Center for Transportation Research, The University of Texas at Austin.
- McCullough, B. F., Dan Zollinger, and Terry Dossey. (1999). Evaluation of the Performance of Texas Pavements Made with Different Coarse Aggregates. Research Report 3925-1, Center for Transportation Research, The University of Texas at Austin.
- McCullough, B.F., Zollinger, D. and Dossey, T., "Evaluation of the performance of Texas pavements made with different coarse aggregates ", Research Report 3925-1F, The Center for Transportation Research, The University of Texas at Austin, 1998.
- Okamoto, P. A., Report on Review of Concrete Fatigue Models, PCA R&D Serial No. 2213, Portland Cement Association, Skokie, IL, 1999.

- Packard, R. G., and S. D. Tayabji. New PCA Thickness Design Procedure for Concrete Highway and Street Pavements. Proceedings, Third International Conference on Concrete Pavement Design, 1985, pp. 225-236.
- Pinto, R., C., A., and Hover, K., C., "Application of Maturity Approach to Setting Times," ACI Materials Journal, Volume 96, Number 6, pp. 686-691, 1999.
- Powers, T.C., "A Discussion of Cement Hydration in Relation to the Curing of Concrete." Proceedings of the Highway Research Board, 27, Washington, D.C., pp. 178-188, 1947.
- Roesler, J. R., and E. J. Barenberg. Effect of Static and Fatigue Cracking on Concrete Strain Measurements. In Transportation Research Record, No. 1684, TRB, National Research Council, Washington, D.C., 1999, pp. 51-60.
- Roesler, J. R., and E. J. Barenberg. Fatigue and Static Testing of Concrete Slabs. Transportation Research Record, No. 1684, TRB, National Research Council, Washington, D.C., 1999, pp. 71-80.
- Schindler, A., Dossey T. and McCullough, B.F., "Temperature Control during Construction to Improve the Long Term Performance of Portland Cement Concrete Pavement ", Research Report 0-1700-2, The Center for Transportation Research, The University of Texas at Austin, 2002.
- Shi, X. P., T. W. Fwa, and S. A. Tan. Flexural Fatigue Strength of Plain Concrete, ACI Materials Journal, V. 90, No. 5, 1993, pp. 435-440
- Stokoe, K. H., II, and J. A. Bay, Rosenblad, B. L., M. R. Murphy, Fults, K. W., and D. C. Chen. Super-Accelerated Testing of a Flexible Pavement with the Stationary Dynamic Deflectometer (SDD). Presented in the 79th Annual Meeting of the Transportation Research Board, Washington, D.C., January, 2000.
- Suh, Y. C., K. Hankins, and B. F. McCullough. (1992). Early-Age Behavior of Continuously Reinforced Concrete Pavement and Calibration of the Failure Prediction Model in the CRCP-7 Program. Report 1244-3, Center for Transportation Research, The University of Texas at Austin.
- Tang, Tianxi, Dan G. Zollinger, and Sanjaya P. Senadheera, "Analysis of Concave Curling in Concrete Slabs," Vol. 119 No. 4, ASCE Journal of Transportation Engineering, July/Aug 1993, pp. 618-633.
- Thompson, M. R., and E. J. Barenberg. NCHRP Report 1-26: Calibrated Mechanistic Structural Analysis Procedure for Pavements-Phase 2, TRB, National Research Council, Washington, D.C., 1992.
- Vepakomma, S., J.H. Jeong, and D.G. Zollinger,. "Characterization of Cracking Restraint at Saw-Cut Joints Using the German Cracking Frame." Transportation Research Record 1813, National Research Council, pp. 28-35. 2002.

- Vesic, A. S., and S. K. Saxena. Analysis of Structural Behavior of Road Test Rigid Pavements. Highway Research Record 291, HRB, National Research Council, Washington, D.C., 1969, pp. 156-158.
- Westman, G., "Concrete Creep and Thermal Stresses," Doctoral Thesis, Luleå University of Technology, Division of Structural Engineering, 301 pp., 1999.
- Won, M. C., K. Hankins, and B. F. McCullough. (1991). Mechanistic Analysis of Continuously Reinforced Concrete Pavements Considering Material Characteristics, Variability, and Fatigue. Report 1169-2, Center for Transportation Research, The University of Texas at Austin.